Asymptotically Stable Walking for Biped Robots: Analysis via Systems with Impulse Effects

J. W. Grizzle, Gabriel Abba and Franck Plestan

Abstract

Biped robots form a subclass of legged or walking robots. The study of mechanical legged motion has been motivated by its potential use as a means of locomotion in rough terrain, as well as its potential benefits to prothesis development and testing. This paper concentrates on issues related to the automatic control of biped robots, and more precisely, its primary goal is to contribute a means to prove asymptotically stable walking in planar, under actuated biped robot models. Since normal walking can be viewed as a periodic solution of the robot model, the method of Poincaré sections is the natural means to study asymptotic stability of a walking cycle. However, due to the complexity of the associated dynamic models, this approach has only been applied successfully to Raibert's one-legged-hopper, and a biped robot without a torso. The principal contribution of the present work is to show that the control strategy can be designed in a way that greatly simplifies the application of the method of Poincaré to a class of biped models, and in fact, to reduce the stability assessment problem to the calculation of a continuous map from a sub-interval of $\mathbb{R}$ to itself. The mapping in question is directly computable from a simulation model. Secondary contributions of the paper include the formulation of the robot model as a system with impulse effects, the extension of the method of Poincaré sections to this class of models, and the use of the analysis methods developed in the paper for the computation of walking cycles that are optimized with respect to energy consumption.

I. Introduction

Mechanical biped locomotion has been studied for well over 30 years. A broad overview of the state of the art until 1990 can be found in [42], [53], [17], along with motivation for studying this class of electro-mechanical systems. The available literature addresses a wide range of topics, from model formulation, efficient means of computing the dynamical equations, relations between mechanical legged locomotion and biological legged locomotion, methods of synthesizing gaits, the mechanical realization of biped robots, and control.

One can distinguish several control design approaches from the literature. By far, the most common approach to control is through the tracking of pre-computed reference trajectories. The trajectories may be determined via analogy, either with biological systems [53], [1], or with simpler, passive[1], mechanical biped systems [34], [51], [52]; they can be generated by an oscillator, such as van der Pol's oscillator [29], or computed through optimization of various cost criteria, such as minimum expended control energy over a walking cycle [9], [10], [13], [45], [44]. Within the context of tracking, many different control methods have been explored, including continuous-time methods based on PID

J.W. Grizzle is with the Control Systems Laboratory, Electrical Engineering and Computer Science Department, University of Michigan, Ann Arbor, MI 48109-2122, Tel: (734)-763-3598, FAX: (734)-763-8041, Email: grizzle@umich.edu.
G. Abba and F. Plestan are with GRAVIR-LSIIT, ENSPS-Université Louis Pasteur-CNRS, Blvd. Sébastien Brant, 67400 Illkirch-Graffenstaden, France, Tel: (0)3-88-65-50-87, Fax: (0)3-88-65-54-89, Email: {Gabriel.Abba,Franck.Plestan}@ensps.u-strasbg.fr
Corresponding author: Prof. Jessy Grizzle

[1]Here, passive is used in the sense that the system is not actuated, but can walk down an inclined plane.

controllers [39], [16], [17], computed torque and sliding mode control [39], [12], [35], [43], [32], or essentially discrete-time methods, based on impulse control [13]. Other control methods have been investigated that do not rely on pre-computed reference trajectories for the angular positions; these include controlling energy, angular momentum, and others [42], [46], [31], [18], [32], [41], [15]. The control design proposed here will not rely on pre-computed reference trajectories.

To date, for the case of a biped robot with a torso, none of the various control approaches have produced a closed-loop system with provable stability properties. Proving stability is the primary goal of this paper. Since regular walking can be viewed as a periodic solution of the robot model, the method of Poincaré sections is the natural means to study asymptotic stability of a walking cycle. However, due to the complexity of the associated dynamic models, this approach has only been applied to Raibert's one-legged-hopper [31], [11], [15], and a biped robot without a torso [51], [18], [49]. One of the principal contributions of the present work is to show that the control strategy can be designed in a way that greatly simplifies the application of the method of Poincaré to a class of biped models.

The stability analysis is built up in several steps. Section II presents the dynamic model of an under actuated biped robot with a torso. The model includes two important parts: a mechanical model that is valid when one leg is touching the ground (supporting the robot) and the other is free (i.e., not touching the walking surface), and an impulse model of the contact event (the swing leg touching the ground). The model used here is representative of many biped models found in the literature [51], [14], [22], [52], [25], [19]. The main contribution of this section is the formulation of the biped model as a nonlinear system with impulse effects [2], [54], which will be the basis for all of the analysis that follows.

The main contribution of Section III is the extension of the method of Poincaré sections to systems with impulse effects. The extension will be done in sufficient generality that it is applicable to more complex robots than the one treated in Section II. Roughly speaking, the method of Poincaré sections entails finding a (local) hyper-plane that is transversal to a candidate periodic motion of a continuous-time system, and then inducing a discrete-time mapping form the plane to itself [40], [30]. The mapping, called the Poincaré return map, is defined by following the evolution of a trajectory of the continuous-time system from a point on the plane to its next intersection with the plane. Periodic motions of the continuous-time system correspond to fixed points of the induced map. In the case of a

biped robot, there is a natural plane to use in the analysis, namely, the constraints corresponding to an impact with the walking surface. The principal result of Section IV is to show that the freedom in the control design can be used to reduce the stability assessment problem via the method of Poincaré to the (numerical) calculation of a continuous map from a sub-interval of $\mathbb{R}$ to itself. This will be achieved with the use of finite-time stabilizing feedback controllers [20], [3], [4], [5]. The mapping in question, which is a restriction of the Poincaré return map, is directly computable from a simulation model of the closed-loop system. Moreover, as will be shown in Section V, the method is sufficiently simple that it can be used in design, for example, to improve the controller's performance, or to optimize the mechanical parameters of the robot itself.

Section VI analyzes the internal behavior of the robot model in closed loop with a finite-time stabilizing controller, as the gain of the controller tends to infinity. Under bounded control gains, the classical zero dynamics of the mechanical part of the robot model are not invariant under the impact model, and hence cannot be used to analyze any of the asymptotic properties of the closed-loop system. However, in the high gain limit, the invariance of the zero dynamics is recovered. This can be used to explain certain properties of the Poincaré map.

It is emphasized that all of the above will be illustrated on one of the simplest possible biped robot models. The robot consists of a torso, hips, and two legs of equal length, with no ankles and no knees. The two legs are actuated. The reason for this choice of model is two fold: firstly, asymptotically stable walking has never been proved for such a model, and thus this simplest problem is still open [14]; secondly, from a pragmatic standpoint, it did not seem advantageous to obscure the main elements of the control approach with the computational complexity of a more complete biped model.

II. A Simple Biped Model

This section introduces the dynamic model of a simple, planar biped robot. The robot consists of a torso, hips, and two legs of equal length, with no ankles and no knees. It thus has five degrees of freedom. Two torques are applied between the legs and the torso, so the system is under actuated. It is assumed that the walking cycle takes place in the sagittal plane. It is further assumed that the walking cycle consists of successive phases of single support (meaning only one leg is touching the ground), with the transition from one leg to another taking place in an infinitesimal length of time

[45], [48], [14]. This assumption entails the use of a rigid model to describe the impact of the swing leg with the ground. The model of the biped robot thus consists of two parts: the differential equations describing the dynamics of the robot during the swing phase, and an impulse model of the contact event. Such models are very common in the field of biped locomotion. The only contribution made here will be the formulation of the model as a nonlinear system with impulse effects [2], [54], which will set up the model for the analysis to follow.

During the swing phase, the stance leg is modeled as a pivot. Between impacts, it is also assumed that the swing leg does not interact with the ground. This a logically weak link in walking models without extensible legs of some sort (either angular or prismatic joints at the"knees"): one is obliged to imagine (postulate) some means for the swing leg to move without touching the ground until the desired moment of contact. The idea of [34] is adopted here: if for one reason or another, a person's knee is immobilized, walking is still possible. The motion consists of flexing the hip and causing the leg to swing out of the plane of forward motion, and into the frontal plane, normal to the direction of motion. This allows the swing leg to clear the ground and be posed in front of the stance leg. Here, it will be further assumed that the swing leg is designed to renter the plane of motion when the angle of the stance leg attains a given value, θ_1^d. Alternate means of achieving leg clearance are discussed in [34], [14].

A. Mechanical (swing phase) model

During the swing phase of the motion, the stance leg is acting as a pivot, and thus there are only three degrees of freedom. The definition of the angular coordinates and the disposition of the masses of the legs, hips and torso are indicated in Figure 1. In particular, note that all masses are lumped, and positive angles are computed clockwise with respect to the indicated vertical lines. Two torques, u_1 and u_2, are applied between the torso and the stance leg, and the torso and the swing leg, respectively. The dynamic model of the robot between successive impacts is easily derived using the method of Lagrange [50]. This results in a standard second order system

$$D(\theta)\ddot{\theta} + C(\theta)\dot{\theta} + G(\theta) = B(\theta)u, \tag{1}$$

where $u = (u_1, u_2)'$, and $\theta = (\theta_1, \theta_2, \theta_3)'$: θ_1 parameterizes the stance leg, θ_2 the swing leg and θ_3 the torso. The matrices D, C, G and B are given in Appendix A.

The second order system (1) can be written in state space form by defining

$$\dot{x} := \frac{d}{dt}\begin{bmatrix} \theta \\ \omega \end{bmatrix} = \begin{bmatrix} \omega \\ D^{-1}(\theta)\left(-C(\theta,\omega)\omega - G(\theta) + Bu\right) \end{bmatrix} =: f(x) + g(x)u, \tag{2}$$

where $\omega := \dot{\theta}$, and $x := (\theta', \omega')'$. The state space for the system will be taken as $\mathcal{X} := \{(\theta', \omega')' \mid \theta \in M,\ \omega \in I\!R^3\}$, where $M = (-\pi, \pi)^3$.

B. Impact model

The impact between the swing leg and the ground is modeled as a contact between two rigid bodies. The standard model[2] from [24] is used. The motion of the robot is only analyzed for the case that the contact of the swing leg with the ground results in no rebound and no slipping of the swing leg, and the stance leg naturally lifting from the ground without interaction [24]. The conditions for these assumptions to be valid will be indicated.

The contact model requires the full five degrees of freedom of the robot. Add Cartesian coordinates $(z_1, z_2)'$ to the end of the stance leg, as indicated in Figure 1. This gives once again a model of the form

$$D_e(q_e)\ddot{q}_e + C_e(q_e, \dot{q}_e)\dot{q}_e + G_e(q) = B_e(q_e)u + \delta F_{\text{ext}} \tag{3}$$

where $q_e = (\theta_1, \theta_2, \theta_3, z_1, z_2)'$ is the set of generalized coordinates and δF^{ext} represents the external forces acting on the robot at the contact point(s). The basic premises in [24] are that: (a) the impact takes place over an infinitesimally small period of time; (b) the external forces during the impact can be represented by impulses; (c) impulsive forces may result in an instantaneous change in the velocities of the generalized coordinates, but the positions remain continuous; and (d) the torques supplied by the actuators are not impulsional. With these assumptions, (3) is "integrated" over the "duration" of the impact to obtain [24]

$$D_e(q_e)(\dot{q}_e^+ - \dot{q}_e^-) = F^{\text{ext}}, \tag{4}$$

where $F^{\text{ext}} := \int_{t^-}^{t^+} \delta F^{\text{ext}}(\tau) d\tau$ is the result of integrating the contact impulse over the impact duration, $\dot{q}_e^+$ is the velocity just after the impact and $\dot{q}_e^-$ is the velocity just before the impact. Since the positions do not change during the impact, $q_e^+ = q_e^-$.

[2]The model is an extension of the work of [6]. This type of rigid contact model is studied as a limit of a non-rigid contact model in [38].

In order to be able to solve for all of the unknowns, the above equations must be augmented with additional equations that proscribe what happens at the two contact ends. According to [24], since the stance leg is assumed to detach from the ground without interaction, the external forces acting at the pivot point are zero. Thus F^{ext} need only consider the external forces at the end of the swing leg. To compute it, let Υ denote the Cartesian-coordinates of the end of the swing leg:

$$\Upsilon(q_e) := \begin{bmatrix} z_1 + r\sin(\theta_1) - r\sin(\theta_2) \\ z_2 + r\cos(\theta_1) - r\cos(\theta_2) \end{bmatrix}. \tag{5}$$

Then

$$F^{\text{ext}} = E' \begin{bmatrix} F_T \\ F_N \end{bmatrix}, \tag{6}$$

where,

$$E := \frac{\partial \Upsilon}{\partial q_e} = \begin{bmatrix} r\cos(\theta_1) & -r\cos(\theta_2) & 0 & 1 & 0 \\ -r\sin(\theta_1) & r\sin(\theta_2) & 0 & 0 & 1 \end{bmatrix}, \tag{7}$$

and F_T,F_N are the tangent and normal forces, respectively, applied at the end of the swing leg.

Equation (4) thus represents five equations and seven unknowns; the unknowns are $\dot{q}_e^+$ and F^{ext}; $\dot{q}_e^-$ is known since it equals $\left(\omega_1^-, \omega_2^-, \omega_3^-, \dot{z}_1^-, \dot{z}_2^-\right)'$, where $\dot{x}^- = 0$ and $\dot{z}^- = 0$ since the stance leg acts as a pivot before impact. An additional set of two equations is obtained from the condition that the swing leg does not rebound nor slip at impact, namely, $\frac{d}{dt}\Upsilon(q_e) = \frac{\partial \Upsilon}{\partial q_e}\dot{q}_e^+ = 0$; that is,

$$E\dot{q}_e^+ = 0. \tag{8}$$

The set of equations (4) and (8) is linear in the unknowns and can be solved for $\dot{q}_e^+$, F_T and F_N. In Appendix A, it is verified that a unique solution always exists. The result of solving (4) and (8) yields an expression for ${\dot{q}_e}^+$ in term of ${\dot{q}_e}^-$, which should then be used to re-initialize the model (2). In order to do this, a change of coordinates is necessary since the former swing leg is now in contact with the ground, while (1) and (2) assume that θ_1 parameterizes the stance leg. The final result is an expression for $x^+ := (\theta^+, \omega^+)$ in terms of $x^- := (\theta^-, \omega^-)$, which is written as

$$x^+ = \Delta(x^-). \tag{9}$$

The function Δ is given in Appendix A. It is also proven in Appendix A that Δ is continuous.

C. Overall model: system with impulse effects

The overall biped model can now be expressed as a system with impulse effects. Assume that the system trajectories possess finite left and right limits, and denote them by $x^-(t) := \lim_{\tau \nearrow t} x(\tau)$ and $x^+(t) := \lim_{\tau \searrow t} x(\tau)$, respectively. The model is then:

$$\Sigma : \begin{cases} \dot{x}(t) &= f(x(t)) + g(x(t))u(t) & x^-(t) \notin S \\ x^+(t) &= \Delta(x^-(t)) & x^-(t) \in S. \end{cases} \tag{10}$$

where $S := \{(\theta, \omega) \in \mathcal{X} \mid \theta_1 = \theta_1^d\}$. The mathematical meaning of a solution of the model will be made precise in Section III. In simple words, a trajectory of the robot is specified by the mechanical model until an impact occurs. Impact occurs when the state "attains" the set S, which represents the walking surface. At this point, the impact with the surface results in a very rapid change in the velocity components of the state vector. The impulse model of the impact compresses the impact event into an instantaneous moment in time, resulting in a discontinuity in the velocities. The ultimate result of the impact model is a new initial condition from which the mechanical model evolves until the next impact. In order for the state not to be obliged to take on two values at the "impact time", the impact event is, roughly speaking, described in terms of the values of the state "just prior to impact" at time "t^-", and "just after impact" at time "t^+". These values are represented by the left and right limits, x^- and x^+, respectively.

For later use, note that S can be expressed as the level set of a function $H : \mathcal{X} \to I\!R$. Define $H(x) = \theta_1^d - \theta_1$, so that $S := \{(\theta, \omega) \in \mathcal{X} \mid H(x) = 0\}$. Moreover, it can be easily checked that for each point $s \in S$, $\frac{\partial H}{\partial x}(s) \neq 0$ This implies that S is a smooth embedded submanifold of $\mathcal{X}$ [26].

III. Method of Poincaré Sections for Systems with Impulse Effects

Nonlinear systems with impulse effects have not been extensively studied. A stability analysis for equilibrium points can be found in [2], [54], using Lyapunov methods. However, a walking cycle clearly corresponds to a non-trivial periodic orbit, and not to an equilibrium solution of the model, and thus the analysis of [2], [54] is not applicable. This section contains the definition of a solution of a system with impulse effects, the definition of a periodic orbit, and Lyapunov stability notions for periodic orbits. With these notions in place, the method of Poincaré sections, an important tool for analyzing the stability properties of periodic orbits in ordinary differential equations, is extended to systems with impulse effects. While the basic method carries over nicely to this new setting, the proof

differs considerably from the standard one in [40], [30], for example. In particular, Section IV will need a version[3] of the Poincaré method that is applicable to continuous, but not Lipschitz continuous, systems. The development will be kept as compact as possible, with all proofs and several lemmas relegated to Appendix B.

A. Basic definitions

A function $\varphi : [t_0, t_f) \to \mathcal{X}$, $t_f \in I\!R \cup \{\infty\}$, $t_f > t_0$, is a *solution*[4] of (10) if 1) $\varphi(t)$ is right continuous on $[t_0, t_f)$, 2) left limits exist at each point of (t_0, t_f), and 3) there exists a closed discrete subset $\mathcal{T} \subset [t_0, \infty)$ such that, a) for every $t \notin \mathcal{T}$, $\varphi(t)$ is differentiable and $\frac{d\varphi(t)}{dt} = f(\varphi(t)) + g(\varphi(t))u(t)$, and b) for $t \in \mathcal{T}$, $\varphi^-(t) \in S$ and $\varphi^+(t) = \Delta(\varphi^-(t))$. The condition that the set of impact times is closed and discrete simply means that there is no "chattering" about an impact point. A solution $\varphi(t)$ of (10) is *periodic* if there exists a finite $T > 0$ such that $\varphi(t+T) = \varphi(t)$ for all $t \in [t_0, \infty)$. A set $\mathcal{O} \subset \mathcal{X}$ is a *periodic orbit* of (10) if $\mathcal{O} = \{\varphi(t) \mid t \geq t_0\}$ for some periodic solution $\varphi(t)$. An orbit is *non-trivial* if it contains more than one point.

In the following, it is assumed that $u(t)$ in (10) is identically zero, so that one may refer to (10) as being time-invariant. It is further assumed that solutions to (10), when they exist, are unique.

A periodic orbit $\mathcal{O}$ is *stable in the sense of Lyapunov* if for every $\epsilon > 0$, there exists an open neighborhood $\mathcal{V}$ of $\mathcal{O}$ such that for every $p \in \mathcal{V}$, there exists a solution $\varphi : [0, \infty) \to \mathcal{X}$ of (10) satisfying $\varphi(0) = p$ and $\text{dist}(\varphi(t), \mathcal{O}) < \epsilon$ for all $t \geq 0$. $\mathcal{O}$ is *attractive* if there exists an open neighborhood $\mathcal{V}$ of $\mathcal{O}$ such that for every $p \in \mathcal{V}$, there exists a solution $\varphi : [0, \infty) \to \mathcal{X}$ of (10) satisfying $\varphi(0) = p$ and $\lim_{t\to\infty} \text{dist}(\varphi(t), \mathcal{O}) = 0$. $\mathcal{O}$ is *asymptotically stable in the sense of Lyapunov* if it is both stable and attractive. From here on, the qualifier, "in the sense of Lyapunov", will be systematically assumed if it is not made explicit.

Finally, assume that in (10), $S = \{x \in \mathcal{X} \mid H(x) = 0\}$, where $H : \mathcal{X} \to I\!R$ is continuously differentiable. A periodic orbit $\mathcal{O}$ is *transversal* to S if its closure intersects S in exactly one point, and for $\bar{x} := \bar{\mathcal{O}} \cap S$, $L_f H(\bar{x}) := \frac{\partial H}{\partial x}(\bar{x}) f(\bar{x}) \neq 0$ (in words, at the intersection, $\bar{\mathcal{O}}$ is not tangent to S, where $\bar{\mathcal{O}}$ is the set closure of $\mathcal{O}$). In the case of the biped robot, a nontrivial periodic orbit transversal to S will also be referred to as a *periodic walking cycle*.

[3]The standard development assumes that the flow is a local diffeomorphism, while, here, it will not even be a homeomorphism.
[4]The definition is based on [54], except that solutions are taken to be right continuous instead of left continuous.

Remark: Note that a periodic orbit of a system with impulse effects may not be a closed set, since, for $t \in \mathcal{T}$, $\varphi^-(t) \notin \mathcal{O}$ (if solutions were assumed to be left continuous, instead of right continuous, then $\varphi^+(t) \notin \mathcal{O}$). Indeed, a periodic orbit is closed if, and only if, $\mathcal{T} = \emptyset$. For a biped robot, a closed periodic orbit would not correspond to walking because there would be no impact with the walking surface.

B. Poincaré's method

The method of Poincaré sections is extended to systems with impulse effects (10), for the case of nontrivial periodic orbits that are transversal to S. This will be done in a certain amount of generality so that a wide class of biped robot models and controllers can be treated. In particular, the finite-time stabilizing controllers of Section IV will require the use of feedbacks that are continuous, but not Lipschitz continuous.

Consider a time-invariant system with impulse effects

$$\Sigma : \left\{ \begin{array}{rcll} \dot{x}(t) & = & f(x(t)) & x^-(t) \notin S \\ x^+(t) & = & \Delta(x^-(t)) & x^-(t) \in S, \end{array} \right. \tag{11}$$

where the state space $\mathcal{X}$ is an open subset of $\mathbb{R}^n$. The hypotheses that will be used in its analysis are listed below. As a point of notation, φ will be used to denote a solution of the system (11), as defined in Section III-A, and φ^f will denote a solution of the associated ordinary differential equation,

$$\dot{x} = f(x). \tag{12}$$

The point of introducing φ^f is that, firstly, a lot is known about solutions of ordinary differential equations with continuous right hand sides [21]; secondly, in view of the first point, it is convenient to prove properties of (11) in term of properties of (12); thirdly, at times in the proofs, it is necessary to extend a solution of (12) "through" S, while this does not make sense for (11) (that is, for the robot, it does not make sense for its "foot to be stuck in the ground").

Hypotheses:

H1) $f(x)$ is continuous on $\mathcal{X}$;

H2) a solution of (12) from a given initial condition is unique and depends continuously on the initial condition;

H3) there exists a differentiable function $H : \mathcal{X} \to I\!R$ such that $S = \{x \in \mathcal{X} \mid H(x) = 0\}$; moreover, for every $s \in S$, $\frac{\partial H}{\partial x}(s) \neq 0$.

H4) $\Delta : S \to \mathcal{X}$ is continuous, where S is given the subset topology from $\mathcal{X}$.

Hypothesis H1 implies that at any point $x_0 \in \mathcal{X}$, a solution to (12) will exist over a sufficiently small interval of time [21]. This solution may not be unique, and may not depend continuously on the initial condition; whence Hypothesis H2. Hypothesis H3 implies that S is an embedded submanifold [26], when given the subset topology. Hypothesis H4 assures that the result of an impact varies continuously with respect to where it occurs on S.

The first goal is to define the Poincaré return map. Define the *time to impact* function, $T_I : \mathcal{X} \to I\!R \cup \{\infty\}$, by

$$T_I(x_0) := \begin{cases} \inf_{t \geq 0}\{\varphi^f(t, x_0) \in S\} & \text{if } \exists\ t \text{ such that } \varphi^f(t, x_0) \in S \\ \infty & \text{otherwise} \end{cases} \tag{13}$$

From Lemma 3 in Appendix B, Hypotheses H1-H3 imply that T_I is continuous at points x_0 where $0 < T_I(x_0) < \infty$ and $L_f H(\varphi^f(T_I(x_0), x_0)) \neq 0$. Hence, under H1-H3, $\tilde{\mathcal{X}} := \{x \in \mathcal{X} \mid 0 < T_I(x) < \infty \text{ and } L_f H(\varphi^f(T_I(x), x)) \neq 0\}$ is open. If H4 also holds, then $\tilde{S} := \Delta^{-1}(\tilde{\mathcal{X}})$ is an open subset of S. It immediately follows that under H1-H4, the *Poincaré return map*, $P : \tilde{S} \to S$ by

$$P(x) := \varphi^f(T_I(\Delta(x)), \Delta(x)), \tag{14}$$

is well-defined and continuous. In the case of the robot, the return map represents the evolution of the robot just before an impact with the walking surface, to just before the next impact, assuming that next impact does occur. If it does not, that is, the robot falls due to the preceeding impact, the point being analyzed is not in the domain of definition of the return map.

Next, note that under H1-H4, if $\mathcal{O}$ is any periodic orbit of (11) that is transversal to S, then $\mathcal{O} \subset \tilde{\mathcal{X}}$. This is essentially by definition. Thus, there exists $x_0 \in \tilde{S}$ that generates $\mathcal{O}$ in the sense that $\Delta(x_0) \in \mathcal{O}$; indeed, $x_0 = \bar{\mathcal{O}} \cap \tilde{S}$. It thus makes sense to denote the orbit by $\mathcal{O}(\Delta(x_0))$.

THEOREM 1 (Method of Poincaré Sections for Systems with Impulse Effects) Under H1-H4, the following statements hold:

a) If $\mathcal{O}$ is a periodic orbit of (11) that is transversal to S, then there exists a point $x_0 \in \tilde{S}$ that generates $\mathcal{O}$.

b) $x_0 \in \tilde{S}$ is a fixed point of P if, and only if, $\Delta(x_0)$ generates a periodic orbit that is transversal to S.

c) $x_0 \in \tilde{S}$ is a stable equilibrium point of $x_{k+1} = P(x_k)$ if, and only if, the orbit $\mathcal{O}(\Delta(x_0))$ is stable in the sense of Lyapunov.

d) $x_0 \in \tilde{S}$ is an asymptotically stable equilibrium point of $x_{k+1} = P(x_k)$ if, and only if, the orbit $\mathcal{O}(\Delta(x_0))$ is asymptotically stable in the sense of Lyapunov.

The proof of the theorem is given in Appendix B.

IV. Asymptotically Stable Walking

This section develops a feedback controller for the system with impulse effects, (10), in the particular case of the biped robot given by the differential equation (2) and the impact model (9). The goal of the control design is to induce an asymptotically stable walking cycle, and to facilitate the verification of its existence and stability properties. The verification will be done using the method of Poincaré. In Section V, the controller design method developed here will be shown to be useful in the search for walking cycles that are (locally) "optimal" with respect to energy consumption, for example, or for which the required torques are "physically reasonable". It is emphasized that, in this section, no attempt is made to optimize anything. The main focus is simply to propose a controller design method for which a set of conditions for asymptotically stable walking can be given, and, in addition, the conditions can be verified in a straightforward manner. In other terms, the reader is asked to be patient if large torques are initially used in the stabilization process, as this *lacuna* will be addressed in the ensuing Section.

A. Encoding a walking pattern

At its most basic level, walking consists of two things [41]: posture control, that is, maintaining the torso in a semi-erect position, and swing leg advancement, that is, causing the swing leg to come from behind the stance leg, pass it by a certain amount, and prepare for contact with the ground. For a "normal" robot with knees, the advancing of the swing leg would also entail preventing it from contacting the walking surface too soon, and causing the robot to trip, whereas for the rigid-legged robot, this issue is moot.

The simplest version of posture control is to maintain the angle of the torso at some constant value, say θ_3^d, while the simplest version of swing leg advancement is to command the swing leg to behave as the mirror image of the stance leg, that is, $\theta_2 = -\theta_1$. Thus the "behavior" of walking will be "encoded"

into the dynamics of the robot by defining outputs

$$y := \begin{bmatrix} y_1 \\ y_2 \end{bmatrix} := \begin{bmatrix} h_1(\theta) \\ h_2(\theta) \end{bmatrix} := \begin{bmatrix} \theta_3 - \theta_3^d \\ \theta_2 + \theta_1 \end{bmatrix}, \tag{15}$$

with the control objective being to drive the outputs to zero. Driving y to zero will force θ_2 and θ_3 to converge to known functions[5] of θ_1 (here, θ_3^d, being a constant, should be viewed as a trivial function of θ_1). This will be one of the key steps in reducing the stability analysis problem to that of a map from $\mathbb{R}$ to $\mathbb{R}$.

Of course, the idea of building in a dynamic behavior of a system through the judicious definition of a set of outputs, which when nulled yields a desireable internal behavior, is not novel in control [26] nor robotics [8], [28], [23], [7], [27], [36], [47]. The result for the biped is essentially to use the system itself as its own trajectory generator, as opposed to tracking pre-computed reference trajectories. This idea seems to be an essential step for *proving* anything about the trajectories of the closed-loop system [8], [7], [36], [47].

B. Controller design

Since the system (2) comes from the second order model (1), and the outputs (15) only depend upon θ, it follows that the relative degree of each output component is either two or infinite. Direct computation gives that [26], [33], [37]

$$\ddot{y} = L_f^2 h(x) + L_g L_f h(x) u \tag{16}$$

and that the determinant of the decoupling matrix, $L_g L_f h$, is (see Appendix A, equation (57))

$$-r\left(rM_H + rm + rM_T + lM_T\cos(\theta_1 - \theta_3)\right).$$

Thus, the decoupling matrix is invertible for all $x \in \mathcal{X}$ as long as $0 < lM_T < r(m + M_T + M_H)$, which imposes a very mild constraint on the position of the center of gravity of the upper body of the robot in relation to the length of its legs. This leads to the following hypothesis.

Hypothesis CH1): The decoupling matrix is globally invertible.

From now on, it is supposed that CH1 is met. Therefore, due to the global invertibility of the decoupling matrix, stabilizing dynamics for the output of system (2) can be assigned. The easiest way

[5]The reason for choosing θ_1 will be clarified in the next Section. The horizontal position of the hips could also have been used as the parameterizing variable; this choice would also work for a robot with knees.

to do this is to first decouple the system [26], [37], [33] and then impose a desired dynamic response. In preparation for doing this, note that $\Phi : M \to \mathbb{R}^3$ by

$$\Phi(\theta) := \begin{bmatrix} y_1 \\ y_2 \\ \theta_1 \end{bmatrix} = \begin{bmatrix} \theta_3 - \theta_3^d \\ \theta_1 + \theta_2 \\ \theta_1 \end{bmatrix} \tag{17}$$

is a diffeomorphism onto its range. With this coordinate transformation, and upon defining

$$v := L_f^2 h + L_g L_f h u, \tag{18}$$

the system can be written in the decoupled-form

$$\begin{bmatrix} \ddot{y} \\ \ddot{\theta}_1 \end{bmatrix} = \begin{bmatrix} v \\ \zeta_0(y, \dot{y}, \theta_1, \dot{\theta}_1) + \zeta_1(y, \dot{y}, \theta_1, \dot{\theta}_1) v. \end{bmatrix} \tag{19}$$

The next step is to impose a continuous feedback $v = v(y, \dot{y})$ on (19), and thus on (10), so that the pair of double integrators $\ddot{y} = v$ is globally finite-time stabilized [20], [3], [4], [5]. This will collapse the image of the Poincaré return map to a one-dimensional set.

Hypotheses: The closed-loop pair of double integrators, $\ddot{y} = v(y, \dot{y})$, satisfies the following conditions:

CH2) solutions globally exist on $\mathbb{R}^4$, and are unique;

CH3) solutions depend continuously on the initial conditions;

CH4) the origin is globally asymptotically stable, and convergence is achieved in finite time;

CH5) the settling time function[6], $T_{set} : \mathbb{R}^4 \to \mathbb{R}$ by

$$T_{set}(y_0, \dot{y}_0) := \inf\{t > 0 \mid (y(t), \dot{y}(t)) = (0,0),\ (y(0), \dot{y}(0)) = (y_0, \dot{y}_0)\}$$

depends continuously on the initial condition, $(y_0, \dot{y}_0)$.

Hypotheses CH2-CH4 correspond to the definition of finite-time stability [20], [3]; CH5 will also be needed, but is not implied by CH2-CH4 [4]. These requirements rule out traditional sliding mode control, with its well-known discontinuous action. A means of meeting these four objectives can be found in [3], [4]. The first two parts of the following lemma are proven in [3]. The continuity of the settling time function is proven in [4] (a continuous upper bound on the settling time function is given in [3], along with a Lyapunov function).

Lemma 1 (Bhat and Bernstein) Consider the double integrator on $\mathbb{R}^2$,

$$\begin{aligned} \dot{x}_1 &= x_2 \\ \dot{x}_2 &= \nu. \end{aligned} \tag{20}$$

[6]That is, the time it takes for a solution initialized at $(y_0, \dot{y}_0)$ to converge to the origin. The terminology is taken from [3].

with scalar input ν. Then, for all $0 < \alpha < 1$, the feedback

$$\nu = \psi_\alpha(x_1, x_2) := -\text{sign}(x_2)|x_2|^\alpha - \text{sign}(\phi_\alpha(x_1, x_2))|\phi_\alpha(x_1, x_2)|^{\frac{\alpha}{2-\alpha}}, \tag{21}$$

where $\phi_\alpha(x_1, x_2) := x_1 + \frac{1}{2-\alpha}\text{sign}(x_2)|x_2|^{2-\alpha}$, satisfies the following:

P1: ν is continuous;

P2: the origin of (20) in closed-loop with (21) is globally finite-time stable;

P3: the settling time function, T_{set}, depends continuously on the initial condition.

Let $\psi_i(x_1, x_2)$, $i = 1, 2$, be any feedbacks for (20) meeting P1-P3 of Lemma 1. To each double integrator of (19), apply the feedback $v_i = \psi_i(y_i, \dot{y}_i)$, so that, with

$$v := \Psi(y, \dot{y}) := \begin{bmatrix} \psi_1(y_1, \dot{y}_1) \\ \psi_2(y_2, \dot{y}_2) \end{bmatrix}, \tag{22}$$

CH2-CH5 are satisfied for $\ddot{y} = v$. Define a feedback on (2), and hence on (10) as well, by

$$u(x) := (L_g L_f h(x))^{-1} \left(\Psi(h(x), L_f h(x)) - L_f^2 h(x)\right), \tag{23}$$

and denote the right-hand side of the closed-loop by

$$f_{cl}(x) := f(x) + g(x)u(x). \tag{24}$$

Finally, define

$$T_{set}^{cl}(x) := \max\{T_{set}(h_1, L_f h_1), T_{set}(h_2, L_f h_2)\} \tag{25}$$

in the obvious way. It follows that $T_{set}^{cl}(x)$ is a continuous function of x.

The model of the biped robot in closed loop with the controller is thus:

$$\Sigma_{cl} : \begin{cases} \dot{x}(t) & = & f_{cl}(x(t)) & x^-(t) \notin S \\ x^+(t) & = & \Delta(x^-(t)) & x^-(t) \in S. \end{cases} \tag{26}$$

In the next subsection, the method of Poincaré sections will be applied to analyze the existence and stability of periodic orbits. The finite-time convergence property of the controller will be exploited to deduce properties of the solutions of (26) by studying the solutions of

$$\dot{x}(t) \quad = \quad f_{cl}(x(t)) \tag{27}$$

corresponding to a one-dimensional subset of initial conditions.

C. Analysis à la Poincaré

The first step in the analysis is to verify that Hypotheses H1-H4 hold for the closed-loop system (26). Lemma 5 of Appendix B shows that continuity of the feedback (22) plus Hypotheses CH1-CH3 imply H1 and H2. Hypotheses H3 and H4 were verified in Section II-C and Section II-B, respectively. Thus Theorem 1 is applicable. The second step in the analysis is to simplify the application of the theorem. This is achieved by studying the image of the Poincaré return map in the case that the controller has had sufficient time to converge. Convergence of the controller is equivalent to the outputs, (15), being identically zero.

The internal dynamics of the system (2) compatible with the output (15) being identically zero is called the zero dynamics [26], and the state space on which the zero dynamics evolves is called the zero dynamics manifold. For the biped model under study, the zero dynamics manifold is computed from (19) to be

$$Z = \left\{ (\theta,\omega) \in \mathcal{X} \mid \theta_3 = \theta_3^d,\ \theta_1+\theta_2 = 0,\ \omega_3 = 0,\ \omega_1+\omega_2 = 0,\ \ -\pi < \theta_1 < \pi,\ \omega_1 \in I\!R \right\}. \tag{28}$$

Note that the feedback (23) makes Z an invariant manifold of (2), while the same feedback does not render Z invariant for (10) since Δ does not map $Z \cap S$ into Z. The zero dynamics itself will not be computed here since it is not needed directly in the stability analysis; the zero-dynamics will be studied in Section VI (see also Appendix A).

Lemma 2: Under Hypotheses CH1-CH5, and H3-H4

1. The set

$$\hat{S} := \{ x_0 \in S \mid T_{set}(x_0) < T_I(x_0) < \infty,\ L_f H(\phi^f(T_I(x_0), x_0)) \neq 0 \} \tag{29}$$

is an open subset of $\tilde{S}$.

2. Let $P : \tilde{S} \to S$ be the Poincaré return map. Then $P : \hat{S} \to S \cap Z$.

The straightforward proof is skipped. Note that in terms of the original coordinates (θ,ω) of the robot,

$$S \cap Z = \left\{ (\theta,\omega) \in \mathcal{X} \mid \theta_3 = \theta_3^d,\ \theta_1+\theta_2 = 0,\ \omega_3 = 0,\ \omega_1+\omega_2 = 0,\ \theta_1 = \theta_1^d,\ \omega_1 \in I\!R \right\},$$

a one-dimensional (embedded) submanifold of $\mathcal{X}$. Define

$$\rho : \hat{S} \cap Z \to S \cap Z \text{ by } \rho(x) := P(x). \tag{30}$$

For $x^* \in \hat{S}$, $P(x^*) \in S \cap Z$. Thus, by the definition of ρ, $P(x^*) = x^*$ if, and only if, $x^* \in \hat{S} \cap Z$ and $\rho(x^*) = x^*$. Suppose that for some $x_0 \in \hat{S}$, the sequence $x_{k+1} := P(x_k)$ is well-defined for $k \geq 0$, and remains in some open neighborhood of x_0. Then for all $k \geq 1$, $x_{k+1} = \rho(x_k)$. It follows that $x^* \in \hat{S}$ is a stable (resp., asymptotically stable) equilibrium point of P if, and only if, it is a stable (resp., asymptotically stable) equilibrium point of ρ. Thus, the determination of the existence and stability properties of periodic orbits that are transversal to $\hat{S}$ can be reduced to the analysis of a one-dimensional map. These results are summarized in the following theorem. A numerical example to the biped robot is given immediately in the next subsection.

THEOREM 2 (Method of Poincaré for Finite-Time Control) Consider the biped robot model of Section II, written in the form of a system with impulse effects, (10). Define outputs such that Hypothesis CH1 is met. Suppose that a continuous, finite-time stabilizing feedback is applied, and that Hypotheses CH2-CH4 are met. Define Z, $\hat{S}$ and ρ as in (28), (29) and (30), respectively. Then,

1. A periodic orbit is transversal to $\hat{S}$ if, and only if, it is transversal to $\hat{S} \cap Z$.
2. $x^* \in \hat{S} \cap Z$ gives rise to a periodic orbit of (26) if, and only if, $\rho(x^*) = x^*$.
3. $x^* \in \hat{S} \cap Z$ gives rise to a stable (resp., asymptotically stable) periodic orbit of (26) if, and only if, x^* is a stable (resp., asymptotically stable) equilibrium point of ρ.

D. Numerical example

Consider the model (10), with the following values of the parameters:

$$m = 5 \quad M_H = 15 \quad M_T = 10 \quad r = 1 \quad l = 0.5$$

corresponding to the mass of the legs, the mass of the hips, the mass of the torso, the length of the legs and the distance between the center of mass of the hips and the center of mass of the torso. The units are kilograms and meters. With the outputs defined as in (15), Hypothesis CH1 is met. Suppose that the desired inclination angle of the torso is $\theta_3^d = \pi/6$ and that impact occurs with the walking surface when $\theta_1^d = \pi/8$. In the feedback (23), suppose that

$$\Psi(x) := \begin{bmatrix} \frac{1}{\epsilon^2}\psi_\alpha(y_1, \epsilon\dot{y}_1) \\ \frac{1}{\epsilon^2}\psi_\alpha(y_2, \epsilon\dot{y}_2) \end{bmatrix} \tag{31}$$

is used, with $\epsilon = 0.1$ and $\alpha = 0.9$, where $\psi_\alpha(x_1, x_2)$ is given by (21). The parameter $\epsilon > 0$ allows the settling time of the controller to be adjusted. With this feedback, CH2-CH5 hold. In the impact

model (9), it is supposed that the friction coefficient $\mu \geq 2/3$ (see Appendix A). In the course of the simulations, it has been verified that the impact model is valid, so this point will not be discussed further.

To determine if this choice of parameters results in an asymptotically stable walking cycle that is transversal to $\hat{S}$, that is, the orbit is transversal to S and the finite-time stabilizing feedback has had enough time to converge over the walking cycle, the function ρ of Theorem 2 must evaluated. This is conveniently done as follows. Define $\sigma : I\!R \to \hat{S} \cap Z$ by $\sigma(\omega_1^-) := (\theta_1^d, -\theta_1^d, \theta_3^d, \omega_1^-, -\omega_1^-, 0)$, where ω_1^- denotes the angular velocity of the stance leg just before impact. Define $\lambda := \sigma^{-1} \circ \rho \circ \sigma$. A straightforward procedure for evaluating λ on the basis of a simulation model of the closed-loop system is now given.

Numerical Procedure to Test for Walking Cycles via the Method of Poincaré:

1) For a point $\omega_1^- > 0$, compute $x^- := \sigma(\omega_1^-)$, the position of the robot just before impact (the restriction to positive velocities corresponds to the robot walking from left to right).

2) Apply the impact model to x^-, that is, compute $x^+ := \Delta(x^-)$.

3) Use x^+ as the initial condition in (27), the robot in closed loop with the controller, and simulate until one of the following happens:

a) there exists a time $T > 0$ where $\theta_1(T) = \theta_1^d$; then, if T is greater than the settling time of the controller (in other words, the output y is identically zero), then $x^+ \in \hat{S} \cap Z$, and $\lambda(\omega_1^-) = \omega_1(T)$; else, $x^+ \notin \hat{S} \cap Z$, and $\lambda(\omega_1^-)$ is undefined at this point.

b) there does not exist a $T > 0$ such that $\theta_1(T) = \theta_1^d$ (which is normally detected by one of the angles exceeding $\pm\pi$ during the simulation); in this case, it is also true that $x^+ \notin \hat{S} \cap Z$, and $\lambda(\omega_1^-)$ is undefined at this point.

Figure 2 displays the function λ; it also displays the related function $\delta\lambda(\omega_1^-) := \lambda(\omega_1^-) - \omega_1^-$, which represents the change in velocity over successive cycles, from just before an impact to just before the next one. It is seen that λ is undefined for ω_1^- less than approximately 1.32 radians/second (for initial ω_1^- less than this value, the robot fell backwards). The plot was truncated at 2 radians/second because nothing interesting occurs beyond this point (except an upper bound on its domain of existence will eventually occur due to the controller not having enough time to settle over one walking cycle). A fixed point occurs at approximately 1.6 radians/second, and, from the graph of λ, it clearly corresponds

to an asymptotically stable walking cycle. Figures 3, 4 and 5 display the states and applied torques of the robot over a few walking cycles, where the initial condition is taken as $(-\frac{1}{2}\theta_1^d, \theta_1^d, \pi/10, 1, 0, 0)$. For reasons of readability of the plots, only a few cycles of walking are shown. Simulation verifies the stability claims of the mathematical analysis.

To illustrate the role played by the inclination of the torso, suppose that θ_3^d is reduced by half to $\pi/12$. Figure 6 displays λ and $\delta\lambda$ for this case. It is seen that there is no fixed point, and hence no periodic orbit that is transversal to $\hat{S}$. Simulations also support this conclusion, but are not reported here for reasons of space. For a robot without knees or ankles, the driving force for walking comes from the inclination of the torso, which couples in the force of gravity.

V. Approximate Optimization in Closed Loop

The goal of this section is to illustrate how Theorem 2 can be used to improve the choice of the output functions made in (15), in order to use less energy over a walking cycle, and/or to reduce the magnitude of the required torques. A reason for seeking to minimize energy consumption is that this will tend to maximize the autonomy of the biped, assuming that it is powered on-board. The results will not be developed in any real generality. Instead, a very concrete illustration in terms of the robot model used in Section IV-D will be pursued. The section starts with a very brief and high-level overview of the existing literature, and then turns quickly to the problem at hand.

A. Background

A significant portion of the research effort in legged motion is aimed at producing walking motions that are energetically optimal in some sense. Often, optimization is used as a means to generate trajectories that correspond to walking with a low consumption of energy per stride, a physically feasible range of applied torques, or even just to find trajectories that correspond to a periodic motion of the model [9], [10], [13], [45], [44]. Classical or modern control methods are then applied to achieve tracking of the so-generated trajectories, and the overall success of the approach is evaluated via simulation or experiment.

Optimization is, in general, numerically very challenging, but the specific problem that is normally posed in order to determine walking trajectories is especially difficult. The difficulty arises from to the necessity to impose boundary conditions that correspond to a periodic solution of the model equations.

The optimization problem thus consists of minimizing a cost function over control inputs and initial conditions, with the constraint that the corresponding solution of the model equations be periodic[7]. Finding feasible solutions has proven to be very difficult, to the point that several studies of the problem have made approximations in the models, such as removing Coriolis terms, setting off-diagonal terms of the inertia matrix to zero, etc. [13], [45]. Such simplifications will not be necessary with the approach outlined in this section.

B. Trajectory parameterization

It is common in the optimization problems treated in the literature to reduce the problem from functional optimization to finite dimensional optimization, with constraints [9], [10], [13], [45]. This is achieved by parameterizing either the inputs, or the trajectories to-be-tracked, in some finite manner, as functions of time. Typically, one uses polynomials, truncated Fourier expansions, or piece-wise constant functions of time. Here, a closely related, but importantly different approach will be taken.

Consider a walking motion of the biped, as illustrated for example in Figures 3 and 4. It is clear that $\theta_1(t)$ is monotonically increasing over each cycle; indeed $\omega_1(t) > 0$ could be considered as part of the requirement of smooth walking, as opposed to standing, or walking with halts during a step. For any periodic trajectories $\theta_2(t)$ and $\theta_3(t)$ that express (encode) a desired walking pattern for the biped, it is thus reasonable to assume that the corresponding trajectory for θ_1 has the property that $\omega_1(t) > 0$ at each instant of time, or equivalently, that $\theta_1(t)$ is strictly monotonic. It follows that $\theta_2(t)$ and $\theta_3(t)$ can each be re-parameterized in terms of θ_1. That is, without loss of generality, it can be supposed that $\theta_3(t) = \eta_1(\theta_1(t))$ and $\theta_2(t) = \eta_2(\theta_1(t))$, for some functions η_i. A finite parameterization is achieved by taking η_i to be polynomials, for example. The outputs selected previously in (15) correspond to $\eta_1(\theta_1) = \theta_3^d$ (a constant) and $\eta_2(\theta_1) = -\theta_1$.

C. Approximate minimization of energy consumption over an asymptotically stable walking cycle

Consider the robot model (10), with parameters and controller as selected in Section IV-D. Let $h_1^a(x) = \theta_3 - \eta_1^a(\theta_1)$ and $h_2^a(x) = \theta_2 - \eta_2^a(\theta_1)$, where each η_i^a is a polynomial in θ_1, and $a = (a_1, \ldots, a_N)$ is a vector of parameters. The objective is to choose the parameter vector a in such a manner that

[7]One sometimes imposes additional conditions related to the length of the stride or the average linear velocity of the walking cycle.

the feedback

$$u(t) := (L_g L_f h^a(x(t)))^{-1} \left(\Psi(x(t)) - L_f^2 h^a(x(t)) \right), \tag{32}$$

with Ψ as in (31), will induce an asymptotically stable walking cycle, and result in lower energy consumption over the walking cycle than the feedback based on (15).

From Theorem 2, a necessary condition for the existence of an asymptotically stable walking cycle is the existence of a pre-impact velocity ω_1^- such that $\lambda(\omega_1^-) > \omega_1^-$. For the biped model as used in Section IV-D, $\lambda(1.55) = 1.574 > 1.55$. Let $\hat{\omega}_1^- := 1.55$. Define a cost function by

$$\hat{J}(a) := \int_0^{\hat{T}} u_1^2(t) + u_2^2(t) dt, \tag{33}$$

where, $\hat{T} := \min\{T_I(\Delta \circ \sigma(\hat{\omega}_1^-)), 2\}$ and $u(t)$ is the result of applying (32) to (10), with initial condition $x_0 := \Delta \circ \sigma(\hat{\omega}_1^-)$ (the upper-bound on $\hat{T}$ is to keep the cost finite for initial conditions not in $\hat{S}$). The cost is an approximation of the average energy consumed over a walking cycle. The goal will be to minimize $\hat{J}(a)$, subject to searching over values of a that will (tend to) give an asymptotically stable closed loop. To do this, the optimization is done subject to constraints $c \leq 0$, where

$$\begin{aligned} c_1 &:= \hat{\omega}_1^- - 0.99\lambda(\hat{\omega}_1^-) \\ c_2 &:= ||y(\bar{t})|| \\ c_3 &:= |F_T/F_N| - \mu \\ c_4 &:= -\dot{z}_2^+, \end{aligned}$$

and $\bar{t}$ is such that $\theta_1(\bar{t}) = \frac{1}{2}\theta_1^d$. The first constraint imposes that there exists a point where $\lambda(\omega_1^-) > \omega_1^-$, helping to assure the existence of a fixed point. The second constraint assures that the finite time controller has converged before impact (so that Theorem 2 is applicable), and the last two constraints assure that the impact model is valid.

This problem was set up and solved in MATLAB using the constrained optimization function `constr`, from the Optimization ToolBox. The functions η_i^a were taken as

$$\eta_1^a(\theta_1) := a_1^0 + \cdots + a_1^3(\theta_1)^3 \tag{34}$$

$$\eta_2^a(\theta_1) := -\theta_1 + (a_2^0 + \cdots + a_2^3(\theta_1)^3) \times (\theta_1 + \theta_1^d) \times (\theta_1 - \theta_1^d). \tag{35}$$

The rather particular form of η_2^a was arrived at by imposing that $h_2^a(\theta_1^d) = h_2^a(-\theta_1^d) = 0$, which is the condition needed for the robot's legs to have equal length at impact (recall the discussion in Section

II-B). The initial and final values of the parameters are shown in Table I, along with the cost. Figure 7 presents the corresponding graph of λ for the optimized value of the output functions. It is seen that there is an asymptotically stable orbit at $\omega_1^- \approx 1.56$. Simulation results support this. Figures 8, 9 and 10 present the corresponding plots of θ, ω and u, respectively, over a few cycles near the stable orbit. Fortuitously, the peak torque magnitude has been reduced to 85 Nm, without explicitly taking this as an objective in the optimization. Finite-time feedbacks with explicit magnitude constraints can also be designed; see [3].

It is possible to pose an optimization problem that more closely reflects the energy used over the walking cycle, and yet is still free of the fixed-point (or two-point boundary value) constraints that have plagued previous approaches to trajectory optimization. For example, for a given value of the parameter vector a, compute a finite-time stabilizing feedback. Evaluate the graph of λ. From this, directly determine whether an asymptotically stable orbit exists or not, and if it does, evaluate the energy consumed over the orbit via

$$J(a) := \int_0^T u_1^2(t) + u_2^2(t) dt, \tag{36}$$

where T is the period of the orbit, and $u(t)$ is the result of (32) over the periodic orbit; else, if an asymptotically stable orbit does not exist, set $J(a) = \infty$. This approach was not followed here due to the increased computational demands, with respect to the previous method.

VI. Analysis of the Zero Dynamics in Relation to High Gain Control

The previous sections have provided an effective method for determining the existence of a periodic orbit, and for analyzing its stability properties. The goal of this section is to analyze more deeply the internal behavior of the robot model in closed loop with a finite-time stabilizing controller. As pointed out in Section IV-C, the classical zero dynamics of the mechanical part of the robot model are not invariant under the impact model, when bounded control gains are used. It is shown here that in the limit as the gain tends to infinity, the invariance of the zero dynamics is recovered, independent of the impact model. This can be used to explain certain properties of the Poincaré map, λ, such as its observed strict monotonicity. For reasons of space, the exposition will be more terse than that of the previous sections.

A. Zero dynamics

It is easy to verify that the input vector fields of (2) commute; that is, their Lie bracket is zero. This, in combination with the decoupling matrix being globally invertible, implies that the dynamic (2), with outputs (15), can be transformed into a particularly simple normal form [26]. An appropriate coordinate transformation can be found by applying Proposition 1.3, page 237, plus the constructive proof of the Frobenius Theorem, page 26, in this same reference. The result is the following change of coordinates, which is a global diffeomorphism under Hypothesis CH1:

$$\bar{x} = \begin{bmatrix} \theta_3 - \theta_3^d \\ \theta_1 + \theta_2 \\ \omega_3 \\ \omega_1 + \omega_2 \\ \omega_1 \\ \gamma(x) \end{bmatrix}, \tag{37}$$

where,

$$\begin{aligned} \gamma(x) \;=\; & \left(\frac{5}{4}mr^2 + M_H r^2 + M_T r^2 - \frac{1}{2}mr^2\cos(\theta_1-\theta_2) + M_T rl\cos(\theta_1-\theta_3)\right)\omega_1 \\ & + \left(\frac{1}{4}mr^2 - \frac{1}{2}mr^2\cos(\theta_1-\theta_2)\right)\omega_2 + \left(M_T l^2 + M_T rl\cos(\theta_1-\theta_3)\right)\omega_3. \end{aligned} \tag{38}$$

The constructive proof of the Frobenius Theorem shows, in fact, that the function γ is the last row of the matrix

$$\left[B, \begin{bmatrix} 0 \\ 0 \\ 1 \end{bmatrix}\right]^{-1} \times D \times \begin{bmatrix} \omega_1 \\ \omega_2 \\ \omega_3 \end{bmatrix}.$$

Note that $(\bar{x}_1, \bar{x}_2, \bar{x}_3, \bar{x}_4) = (h_1(x), h_2(x), L_f h_1(x), L_f h_2(x))$.

In the $\bar{x}$-coordinates, the state space model of the robot, (2), with the decoupling feedback, (18), becomes

$$\dot{\bar{x}} = \begin{bmatrix} \bar{x}_3 \\ \bar{x}_4 \\ v_1 \\ v_2 \\ \dfrac{4M_T l\left(r\cos(\bar{x}_1 - \bar{x}_5 + \theta_3^d) - l\right)\bar{x}_3 + mr^2\left(2\cos(\bar{x}_2 - 2\bar{x}_5) - 1\right)\bar{x}_4 + 4\bar{x}_6}{4r\left(mr + M_H r + M_T r + M_T l\cos(\bar{x}_1 - \bar{x}_5 + \theta_3^d)\right)} \\ g\left(M_T l\sin(\bar{x}_1 + \theta_3^d) - \frac{1}{2}mr\sin(\bar{x}_2 - \bar{x}_5) + \left(\frac{3}{2}mr + M_T r + M_H r\right)\sin(\bar{x}_5)\right) \end{bmatrix}. \tag{39}$$

The zero dynamics is obtained by imposing $y(t) \equiv 0$. Setting $(\bar{x}_1, \bar{x}_2, \bar{x}_3, \bar{x}_4) = (0, 0, 0, 0)$ in (39), and

relabeling $\bar{x}_5$ and $\bar{x}_6$ by ξ_1 and ξ_2, respectively, yields

$$\begin{bmatrix} \dot{\xi}_1 \\ \dot{\xi}_2 \end{bmatrix} = \begin{bmatrix} \xi_2 \\ \hline r\Big(mr + M_H r + M_T r + M_T l\cos(-\xi_1 + \theta_3^d)\Big) \\ g\Big(M_T l\sin(\theta_3^d) + (mr + M_T r + M_H r)\sin(\xi_1)\Big) \end{bmatrix}. \tag{40}$$

In order to establish the relation between (39) and (40), some properties of a double integrator in feedback with a finite-time converging controller are needed.

B. Aside on the double integrator

Consider a scalar double integrator, $\ddot{\eta}(t) = \nu$, and let $\nu := \psi(\eta, \dot{\eta})$ be any feedback so that Properties P1-P3 of Lemma 1 hold. Let T_{set} be the settling time function and let $\varphi(t, \dot{\eta}_0)$ denote the solution of the closed-loop system corresponding to the initial condition $(0, \dot{\eta}_0)$. By continuity of the dependence of the solution on the initial conditions, and the fact that φ has bounded support[8],

$$\lim_{\epsilon \searrow 0} \sup_{t \geq 0} |\varphi(t, \epsilon\dot{\eta}_0)| = 0 \tag{41}$$

$$\lim_{\epsilon \searrow 0} \sup_{t \geq 0} |\dot{\varphi}(t, \epsilon\dot{\eta}_0)| = 0. \tag{42}$$

Since $\dot{\varphi}$ is a continuous function of t, and has bounded support, $\int_0^\infty |\dot{\varphi}(t, \dot{\eta}_0)|dt$ exists and is finite. Hence, using (42) and the bounded support property, it follows that

$$\lim_{\epsilon \searrow 0} \int_0^\infty |\dot{\varphi}(t, \epsilon\dot{\eta}_0)|dt = \lim_{\epsilon \searrow 0} \int_0^{Tset(0, \epsilon\dot{\eta}_0)} |\dot{\varphi}(t, \epsilon\dot{\eta}_0)|dt = \lim_{\epsilon \searrow 0} \int_0^1 |\dot{\varphi}(t, \epsilon\dot{\eta}_0)|dt = 0. \tag{43}$$

Consider again the scalar double integrator, let $\epsilon > 0$, and apply the high gain feedback $\nu = \frac{1}{\epsilon^2}\psi(\eta, \epsilon\dot{\eta})$. Let $\varphi_\epsilon(t, \dot{\eta}_0)$ denote the solution for the initial condition $(0, \dot{\eta}_0)$. Then it is straightforward to verify that $\varphi_\epsilon(t, \dot{\eta}_0) = \varphi(t/\epsilon, \epsilon\dot{\eta}_0)$, and thus that $\dot{\varphi}_\epsilon(t, \dot{\eta}_0) = \frac{1}{\epsilon}\dot{\varphi}(t/\epsilon, \epsilon\dot{\eta}_0)$. Hence, by (41),

$$\lim_{\epsilon \searrow 0} \sup_{t \geq 0} |\varphi_\epsilon(t, \dot{\eta}_0)| = 0, \tag{44}$$

and by (43) and a simple substitution of variables,

$$\lim_{\epsilon \searrow 0} \int_0^\infty |\dot{\varphi}_\epsilon(t, \dot{\eta}_0)|dt = 0. \tag{45}$$

C. High gain control and the zero dynamics

Once again, let $v_i = \psi_i(y_i, \dot{y}_i)$, $i = 1, 2$, be any feedbacks for the double integrator so that Properties P1-P3 hold. For any $\epsilon > 0$, a simple time scale argument shows that the high gain feedback $v_i =$

[8]Indeed, the support is $[0, T_{set}(0, \epsilon\dot{\eta}_0)]$.

$\frac{1}{\epsilon^2}\psi_i(y_i, \epsilon\dot{y}_i)$ still results in Properties P1-P3 being met, and, furthermore, results in the closed-loop settling time function, (25), becoming $T^{cl}_{set}(y, \dot{y}, \epsilon) = \epsilon T^{cl}_{set}(y, \epsilon\dot{y})$. With this in mind, apply the feedback

$$v := \Psi(\bar{x}) := \begin{bmatrix} \frac{1}{\epsilon^2}\psi_1(\bar{x}_1, \epsilon\bar{x}_3) \\ \frac{1}{\epsilon^2}\psi_2(\bar{x}_2, \epsilon\bar{x}_4) \end{bmatrix}, \tag{46}$$

to (39).

The relationship between the solutions of the closed loop robot model, (39), and the zero dynamics, (40), is established as follows. Take a point $\bar{x}^- \in \hat{S} \cap Z$. Let $\bar{x}^+ := \bar{\Delta}(\bar{x}^-)$, where $\bar{\Delta}$ is the representation of Δ in the coordinates (37). It follows that $\bar{x}^+_1 = 0$ and $\bar{x}^+_2 = 0$, because (15) is identically zero on S. Hence the analysis of Section VI-B is applicable. Letting $\bar{x}(t, \bar{x}^+)$ denote the solution of (39) for the initial condition $\bar{x}^+$, (44) and (45) imply, respectively,

$$\lim_{\epsilon \searrow 0} \sup_{t \geq 0} |\bar{x}_i(t, \bar{x}^+)| = 0, \ \ i = 1, 2, \tag{47}$$

and,

$$\lim_{\epsilon \searrow 0} \int_0^\infty |\bar{x}_j(t, \bar{x}^+)| dt = \lim_{\epsilon \searrow 0} \int_0^{\epsilon T^{cl}_{set}(0,0,\epsilon\bar{x}^+_3, \epsilon\bar{x}^+_4)} |\bar{x}_j(t, \bar{x}^+)| dt = 0, \ \ j = 3, 4. \tag{48}$$

From these two equations, and the fact that $\bar{x}_3$ and $\bar{x}_4$ appear affinely in the fifth row of (39), and not at all in the last row, a simple bounding argument[9] shows that, for $t > 0$,

$$\lim_{\epsilon \searrow o} \bar{x}(t, \bar{x}^+) = \Big(0, 0, 0, 0, \xi_1(t, \bar{x}^+_5, \bar{x}^+_6), \xi_2(t, \bar{x}^+_5, \bar{x}^+_6)\Big)', \tag{49}$$

where $\xi_i(t, \bar{x}^+_5, \bar{x}^+_6)$, $i = 1, 2$, denotes the solution of the zero dynamics, (40), for the initial condition $(\bar{x}^+_5, \bar{x}^+_6)'$.

D. λ under high gain control

It follows that in the high gain limit, that is, as ϵ tends to zero in (46), the function λ from the Poincaré method can be evaluated on the basis of a two dimensional subsystem, namely, the zero dynamics. Denote the result by λ_{HG}. This reduction is interesting for several reasons:

(1) it brings out the structure of the closed-loop system, and shows that the zero dynamics must encode the notion of a walking cycle;

(2) the uniqueness of the solutions of the zero dynamics implies that λ_{HG} is strictly monotonic, which partly explains the observed monotonicity in λ;

[9]Express the solutions in integral form, compute the norm of their difference, and apply the triangle inequality.

3) λ_{HG} is as smooth as the data in the problem (for the biped, it is analytic), whereas λ is only continuous;

(4) the evaluation of λ_{HG} is independent of the particular finite-time stabilizing feedback used. Moreover, it can also be computed by replacing ψ_i in (46) with a globally exponentially stabilizing feedback, and taking the limit as ϵ tends to zero; in the limit, the Poincaré return map, P, when restricted to $\hat{S} \cap Z$, takes again its values in $S \cap Z$. The consequences of this observation for the study of periodic orbits under non-finite-time stabilizing feedback control remain to be clarified.

VII. Conclusions and Perspectives

This paper has addressed the problem of establishing the existence of a periodic orbit in a simple biped model, and analyzing its stability properties. The biped model was first formulated as a nonlinear system with impulse effects, evolving in a subset of $\mathbb{R}^6$. Poincaré's method was then extended to this class of systems. For the biped model considered here, a straightforward application of Poincaré's method would require the computation of a discrete-time map from $\mathbb{R}^5$ to $\mathbb{R}^5$, which would be a complicated task. It was then shown that finite-time converging feedbacks could be used to drive the torso and the swing leg to known functions of the support leg, and thereby collapse the dimension of the image of the Poincaré map to a one-dimensional set. This led to an effective analysis tool, which then could be used in design. In the course of the development of these results, it was observed that the zero dynamics of the biped was not invariant under the impact model. It was subsequently shown that its invariance could be recovered under high gain control.

The analysis method developed in the paper is quite general. The next step is to apply it to a more general biped model with knees [39], [19], [16], [17], yielding a seven degree of freedom, under actuated system. It is conjectured that supplementing outputs (15) with hip height and swing foot height objectives will lead to a viable control design with provable stability properties; the horizontal hip position will play the role of θ_1 in parameterizing the outputs to be used in the feedback design. It also seems likely that the methods developed here can be applied to other under actuated mechanical systems [36].

The work presented here has assumed a rigid impact model. Non-rigid models have been developed [45] in the context of biped motion. It seems possible that some of the results of the paper can be

extended to include such models, though this is more speculative than the previous extension. Finally, many challenging issues exist in running (which has a fly phase) and three dimensional aspects of modeling and control of mechanical biped motion.

Acknowledgments

J.W. Grizzle thanks Dan Koditschek for stimulating conversations on the control of under actuated mechanical systems. This work was initiated while J.W. Grizzle was on sabbatical leave at GRAVIR-LSIIT; he thanks Professor E. Ostertag for his kind hospitality. The work of J.W. Grizzle was supported in part by an NSF GOALI grant, ECS-9631237, and in part by matching funds from Ford Motor Company.

References

[1] R. McN. Alexander. Three uses for springs in legged locomotion. *The International Journal of Robotics Research*, 9(2):53–61, 1990.

[2] D.D. Bainov and P.S. Simeonov. *Systems with Impulse Effects : Stability, Theory and Applications*. Ellis Horwood Limited, Chichester, 1989.

[3] S.P. Bhat and D.S. Bernstein. Continuous finite-time stabilization of the translational and rotational double integrators. *IEEE Transactions on Automatic Control*, 43(5):678–682, 1998.

[4] S.P. Bhat and D.S. Bernstein. Finite-time stability of continuous autonomous systems. *Preprint*, 1998.

[5] S.P. Bhat and D.S. Bernstein. Finite-time stability of homogeneous systems. *Preprint*, 1998.

[6] R.M. Brach. Rigid body collisions. *Journal of Applied Mechanics*, 56:133–138, 1989.

[7] M. Bühler, D. E. Koditschek, and P. J. Kindlmann. Planning and control of a juggling robot. *International Journal of Robotics Research*, 13(2):101–118, 1994.

[8] M. Bühler, D. E. Koditschek, and P.J. Kindlmann. A family of robot control strategies for intermittent dynamical environments. *IEEE Control Systems Magazine*, 10:16–22, Feb 1990.

[9] G. Cabodevilla, G. Abba, and H. Sage. Energetically near optimal gait for a biped robot with double supporting phases. In *Proc. of the Third France-Japan Congress and First Europe-Asia Congress on Mechatronics, Besancon, France*, pages 958–961, October 1996.

[10] G. Cabodevilla, N. Chaillet, and G. Abba. Energy-minimized gait for a biped robot. In *Autonome Mobile Systeme*, pages 90–99. Springer-Verlag, 1995.

[11] C. Canudas, L. Roussel, and A. Goswani. Periodic stabilization of a 1-dof hopping robot on nonlinear compliant surface. In *Proc. of IFAC Symposium on Robot Control, Nantes, France*, pages 405–410, September 1997.

[12] N. Chaillet, G. Abba, and E. Ostertag. Double dynamic modelling and computed-torque control of a biped robot. In *Proc. of the IEEE/RSJ International Conference on Intelligent Robots and Systems, Munich, Germany*, pages 1149–1153, September 1994.

[13] C. Chevallereau, A. Formal'sky, and B. Perrin. Control of a walking robot with feet following a reference trajectory derived from ballistic motion. In *Proc. of the IEEE International Conference on Robotics and Automation, Albuquerque, N.M.*, pages 1094–1099, April 1997.

[14] B. Espiau and A. Goswani. Compass gait revisited. In *Proc. of the IFAC Symposium on Robot Control, Capri, Italy*, pages 839–846, September 1994.

[15] C. Francois and C. Samson. A new approach to the control of the planar one-legged hopper. *The International Journal of Robotics Research*, 17(11):1150–1166, 1998.

[16] J. Furusho and M. Masubuchi. Control of a dynamical biped locomotion system for steady walking. *Journal of Dynamic Systems, Measurement, and Control*, 108:111–118, 1986.

[17] J. Furusho and A. Sano. Sensor-based control of a nine-link biped. *The International Journal of Robotics Research*, 9(2):83–98, 1990.

[18] A. Goswani, B. Espiau, and A. Keramane. Limit cycles and their stability in a passive bipedal gait. In *Proc. of the IEEE International Conference on Robotics and Automation, Minneapolis, MN.*, pages 246–251, April 1996.

[19] A.A. Grishin, A.M. Formal'sky, A.V. Lensky, and S.V. Zhitomirsky. Dynamical walking of a vehicle with two telescopic legs controlled by two drives. *The International Journal of Robotics Research*, 13(2):137–147, 1994.

[20] V.T. Haimo. Finite time controllers. *SIAM J. Control and Optimization*, 24(4):760–770, 1986.

[21] P. Hartman. *Ordinary Differential Equations*. Birkhauser, Boston, 2nd edition, 1982.

[22] H. Hemami and B.F. Wyman. Modeling and control of constrained dynamic systems with application to biped locomotion in the frontal plan. *IEEE Transactions on Automatic Control*, 24(4):526–535, 1979.

[23] Y. Hurmuzlu. Dynamics of bipedal gait - part 1: objective functions and the contact event of a planar five-link biped. *Journal of Applied Mechanics*, 60:331–336, June 1993.
[24] Y. Hurmuzlu and D.B. Marghitu. Rigid body collisions of planar kinematic chains with multiple contact points. *The International Journal of Robotics Research*, 13(1):82–92, 1994.
[25] Y. Hurmuzlu and D. Moskowitz. The role of impact in the stability of bipedal locomotion. *Dynamics and Stability of Systems*, 1(3):217–234, 1986.
[26] A. Isidori. *Nonlinear Control Systems: An Introduction*. Springer-Verlag, Berlin, 2nd edition, 1989.
[27] S. Kajita and K. Tani. Experimental study of biped dynamic walking in the linear inverted pendulum mode. In *Proc. of the IEEE International Conference on Robotics and Automation, Nagoya, Japan*, pages 2885–2891, May 1995.
[28] S. Kajita, T. Yamaura, and A. Kobayashi. Dynamic walking control of biped robot along a potential energy conserving orbit. *IEEE Transactions on Robotics and Automation*, 8(4):431–437, August 1992.
[29] R. Katoh and M. Mori. Control method of biped locomotion giving asymptotic stability of trajectory. *Automatica*, 20(4):405–414, 1984.
[30] H.K. Khalil. *Nonlinear systems - 2nd Edition*. Prentice Hall, Upper Saddle River, 1996.
[31] D.D. Koditschek and M. Buhler. Analysis of a simplified hopping robot. *The International Journal of Robotics Research*, 10(6):587–605, 1991.
[32] N. Manamani, N.N. Gauthier, and N.K. M'Sirdi. Sliding mode control for pneumatic robot leg. In *Proc. of the European Control Conference, Bruxelles, Belgium*, July 1997.
[33] T. Marino and P. Tomei. *Nonlinear Control Design*. Prentice Hall, London, 1995.
[34] T. McGeer. Passive dynamic walking. *The International Journal of Robotics Research*, 9(2):62–82, 1990.
[35] K. Mitobe, N. Mori, K. Aida, and Y. Nasu. Nonlinear feedback control of a biped walking robot. In *Proc. of the IEEE International Conference on Robotics and Automation, Nagoya, Japan*, pages 2865–2870, May 1995.
[36] J. Nakanishi, T. Fukuda, and D.E. Koditschek. Preliminary studies of a second generation brachiation robot controller. In *Proc. of the IEEE International Conference on Robotics and Automation, Albuquerque, N.M.*, pages 2050–2056, April 1997.
[37] H. Nijmeijer and van der Schaft,A. J. *Nonlinear Dynamical Control Systems*. Springer-Verlag, Berlin, 1989.
[38] P. Orhant. *Contribution à la manipulation fine: étude de la phase d'impact*. PhD thesis, Institut National Polytechnique - Grenoble - France, December 1994.
[39] J.H. Park and K.D. Kim. Biped robot walking using gravity-compensated inverted pendulum mode and computed torque control. In *Proc. of the IEEE International Conference on Robotics and Automation, Leuven, Belgium*, pages 3528–3533, May 1998.
[40] T.S. Parker and L.O. Chua. *Practical numerical algorithms for chaotic systems*. Springer-Verlag, New York, 1989.
[41] J. Pratt and G. Pratt. Intuitive control of a planar bipedal walking robot. In *Proc. of the IEEE International Conference on Robotics and Automation, Leuven, Belgium*, pages 2014–2021, May 1998.
[42] M.H. Raibert. Legged robots. *Communications of the ACM*, 29(6):499–514, 1986.
[43] M.H. Raibert, S. Tzafestas, and C. Tzafestas. Comparative simulation study of three control techniques applied to a biped robot. In *Proc. of the IEEE International Conference on Systems, Man and Cybernetics Systems Engineering in the Service of Humans, Le Touquet, France*, pages 494–502, October 1993.
[44] M. Rostami and G. Bessonnet. Impactless sagittal gait of a biped robot during the single support phase. In *Proc. of the IEEE International Conference on Robotics and Automation, Leuven, Belgium*, pages 1385–1391, May 1998.
[45] L. Roussel. *Génération de trajectoires de marche optimales pour un robot bipède*. PhD thesis, Institut National Polytechnique - Grenoble - France, November 1998.
[46] A. Sano and J. Furusho. Realization of natural dynamic walking using the angular momentum information. In *Proc. of the IEEE International Conference on Robotics and Automation, Cincinnati, OH.*, pages 1476–1481, May 1990.
[47] Ulucs Saranli, William J. Schwind, and Daniel E. Koditschek. Toward the control of a multi-jointed, monoped runner. In *IEEE Int. Conf. on Rob. and Aut.*, pages 2676–2682, Leuven, Belgium, May 1998.
[48] C.L. Shih and W.A. Gruver. Control of a biped robot in the double-support phase. *IEEE Transactions on Systems, Man, and Cybernetics*, 22(4):729–735, 1992.
[49] A.C. Smith and M.D. Berkemeier. The motion of a finite-width wheel in 3d. In *Proc. of the IEEE International Conference on Robotics and Automation, Leuven, Belgium*, pages 2345–2350, May 1998.
[50] M.W. Spong and M. Vidyasagar. *Robot dynamics and control*. John Wiley and Sons, New York, 1989.
[51] B. Thuilot, A. Goswani, and B. Espiau. Bifurcation and chaos in a simple passive bipedal gait. In *Proc. of the IEEE International Conference on Robotics and Automation, Albuquerque, N.M.*, pages 792–798, April 1997.
[52] R.Q. van der Linde. Active leg compliance for passive walking. In *Proc. of the IEEE International Conference on Robotics and Automation, Leuven, Belgium*, pages 2339–2344, May 1998.
[53] M. Vukobratovic, B. Borovac, D. Surla, and D. Stokic. *Biped locomotion*. Springer-Verlag, Berlin, 1990.
[54] H. Ye, A.N. Michel, and L. Hou. Stability theory for hybrid dynamical systems. *IEEE Transactions on Automatic Control*, 43(4):461–474, 1998.

VIII. Appendix A: Model Details

This appendix completes the equations of the biped model, (1). In the following, $\omega := \dot{\theta}$.

Mechanical model

$$D = \begin{bmatrix} (\frac{5}{4}m + M_H + M_T)r^2 & -\frac{1}{2}mr^2\cos(\theta_1 - \theta_2) & M_T rl\cos(\theta_1 - \theta_3) \\ -\frac{1}{2}mr^2\cos(\theta_1 - \theta_2) & \frac{1}{4}mr^2 & 0 \\ M_T rl\cos(\theta_1 - \theta_3) & 0 & M_T l^2 \end{bmatrix} \tag{50}$$

$$C = \begin{bmatrix} 0 & -\frac{1}{2}mr^2 s_{12}\omega_2 & M_T rls_{13}\omega_3 \\ \frac{1}{2}mr^2 s_{12}\omega_1 & 0 & 0 \\ -M_T rls_{13}\omega_1 & 0 & 0 \end{bmatrix} \tag{51}$$

$$s_{1j} := \sin(\theta_1 - \theta_j), j \in \{2, 3\} \tag{52}$$

$$G = \begin{bmatrix} -\frac{1}{2}g\left(2M_H + 3m + 2M_T\right)r\sin(\theta_1) \\ \frac{1}{2}gmr\sin(\theta_2) \\ -gM_T l\sin(\theta_3) \end{bmatrix} \tag{53}$$

$$B = \begin{bmatrix} -1 & 0 \\ 0 & -1 \\ 1 & 1 \end{bmatrix} \tag{54}$$

Impact model

The impact equations (4) and (8), taken together, become

$$\begin{bmatrix} D_e & -E' \\ E & 0 \end{bmatrix} \begin{bmatrix} \dot{q}_e^+ \\ F \end{bmatrix} = \begin{bmatrix} D_e\dot{q}_e^- \\ 0 \end{bmatrix}, \tag{55}$$

where, $F = (F_T, F_N)'$ and the positive definite, symmetric matrix D_e has entries

$$\begin{array}{ll} D_e^{11} = \frac{1}{4}\left(5m + 4M_H + 4M_T\right)r^2 & D_e^{12} = -\frac{1}{2}mr^2\cos(-\theta_1 + \theta_2) \\ D_e^{13} = M_T rl\cos(\theta_1 - \theta_3) & D_e^{14} = \frac{1}{2}\left(3m + 2M_H + 2M_T\right)r\cos(\theta_1) \\ D_e^{15} = -\frac{1}{2}\left(3m + 2M_H + 2M_T\right)r\sin(\theta_1) & D_e^{22} = \frac{1}{4}mr^2 \\ D_e^{23} = 0 & D_e^{24} = -\frac{1}{2}mr\cos(\theta_2) \\ D_e^{25} = \frac{1}{2}mr\sin(\theta_2) & D_e^{33} = M_T l^2 \\ D_e^{34} = M_T l\cos(\theta_3) & D_e^{35} = -M_T l\sin(\theta_3) \\ D_e^{44} = 2m + M_H + M_T & D_e^{45} = 0 \\ D_e^{55} = 2m + M_H + M_T & \end{array}$$

The solvability of (55) is equivalent to the invertibility of the matrix on the left hand side. The invertibility of this matrix follows from the fact that D_e is positive definite and E has full rank; indeed, the determinant of the left hand side of (55) can be computed to be

$$\frac{mM_T l^2 r^4}{16}\left(2M_T + 3m + 4M_H - 2m\cos(2\theta_1 - 2\theta_2) - 2M_T\cos(2\theta_2 - 2\theta_3)\right),$$

which is non-zero everywhere.

The mapping Δ is then evaluated by the following steps:

Step 1: solve (55) for $\dot{q}_e^+$, and pick-off ω^+; since $\dot{q}_e^-$ only depends on ω^- (recall that $\dot{z}_1^- = \dot{z}_2^- = 0$), and since the positions do not change during the impact (i.e, $\theta^+ = \theta^-$), the result is ω^+ expressed as a function of $x^- = (\theta^{-\prime}, \omega^{-\prime})'$.

Step 2: transform the coordinates so that θ_1 corresponds to the stance leg and θ_2 to the swing leg; this means swapping the first two position coordinates, and the first two velocity coordinates, respectively. The final result is

$$\Delta(x^-) := \begin{bmatrix} \theta_2^- \\ \theta_1^- \\ \theta_3^- \\ \omega_2^+(x^-) \\ \omega_1^+(x^-) \\ \omega_3^+(x^-) \end{bmatrix} \tag{56}$$

The implicit function theorem implies that Δ is as smooth as the data in (55), and thus Δ is analytic in x^-.

Remarks: (a) Computing Δ in closed form would mean inverting a 7×7 matrix; hence this is only done numerically, as part of the simulations. (b) The no-rebound, no-slip condition of the impact, (8), ensures that the impact results in the end of the swing leg being at rest, and hence, after doing the coordinate transformation, the end of the stance leg will be at rest. (c) For the impact model to be valid, it must be verified *a posteriori* that no-slipping was a valid assumption (that is, $|F_T/F_N| \leq \mu$), and that the stance leg lifts from the ground without interaction (that is, before the coordinate transformation, $\dot{z}_2^+ > 0$). This was done for all simulations reported in this paper.

Decoupling matrix

The Lie derivative notation is defined in [26], [33], [37].

$$L_g L_f h = \frac{1}{\det(D)} \begin{bmatrix} R_{11} & R_{12} \\ R_{21} & R_{22} \end{bmatrix} \tag{57}$$

where,

$$\begin{aligned}
R_{11} &= \frac{mr^3}{16}\Big(5mr + 4M_H r + 4M_T r - 4mr\cos^2(-\theta_1+\theta_2) + 4M_T l\cos(-\theta_1+\theta_3)\Big) \\
R_{12} &= \frac{mr^3}{16}\Big(5mr + 4M_H r + 4M_T r - 4mr\cos^2(-\theta_1+\theta_2) + 8M_T l\cos(-\theta_1+\theta_2)\cos(-\theta_1+\theta_3)\Big) \\
R_{21} &= \frac{-mM_T l r^2}{4}\left(1+2\cos(-\theta_1+\theta_2)\right)\left(r\cos(-\theta_1+\theta_3)+l\right)
\end{aligned}$$

$$R_{22} = \frac{-M_T l r^2}{4}\left(5ml + 4M_H l + 4M_T l + mr\cos(-\theta_1+\theta_3) + 2mr\cos(-\theta_1+\theta_2)\cos(-\theta_1+\theta_3)\right.$$
$$\left.-4M_T l\cos^2(-\theta_1+\theta_3) + 2ml\cos(-\theta_1+\theta_2)\right),$$

and

$$\det(D) = \frac{mM_T r^4 l^2}{16}\left(5m + 4M_H + 4M_T - 4m\cos^2(-\theta_1+\theta_2) - 4M_T\cos^2(-\theta_1+\theta_3)\right).$$

Zero Dynamics

In the coordinates used in (19), the zero dynamics is given by

$$\ddot{\theta}_1 = \zeta_0(0,0,\theta_1,\dot{\theta}_1) =: \bar{\zeta}_a(\theta_1) + \bar{\zeta}_b(\theta_1)\dot{\theta}_1^2, \tag{58}$$

where,

$$\bar{\zeta}_a(\theta_1) = \frac{g}{r}\frac{(2m+M_T+M_H)r\sin(\theta_1) + M_T l\sin(\theta_3^d)}{mr + M_H r + M_T r + M_T l\cos(\theta_1-\theta_3^d)} \tag{59}$$

$$\bar{\zeta}_b(\theta_1) = \frac{M_T l\sin(\theta_1-\theta_3^d)}{mr + M_H r + M_T r + M_T l\cos(\theta_1-\theta_3^d)}. \tag{60}$$

IX. Appendix B: Proofs and Technical Details

This appendix collects some of the technical development, in the hope of improving the readability of the main body of the paper.

Continuity of T_I

Lemma 3: Suppose that Hypotheses H1-H3 hold. Then T_I is continuous at points x_0 where $0 < T_I(x_0) < \infty$ and $L_f H(\varphi^f(T_I(x_0), x_0)) \neq 0$.

Proof: Let $\epsilon > 0$ be given. Define $\bar{x} := \varphi^f(T_I(x_0), x_0)$, and without loss of generality, suppose that $L_f H(\bar{x}) < 0$. Then, from the definition of T_I and H3, $H(\varphi^f(t, x_0)) > 0$ for all $0 \leq t < T_I(x_0)$. This in turn implies that, for any $0 < t_1 < T_I(x_0)$,

$$\mu(t_1) := \inf_{0\leq t\leq t_1} \mathrm{dist}(\varphi^f(t,x_0), S) > 0, \tag{61}$$

since: (a) $\varphi^f(t,x_0)$ is continuous in t; (b) the interval $[0,t_1]$ is compact; and (c), by H3, S is closed and equals the zero level set of H. By H1, there exists $\bar{\epsilon} > 0$ such that φ^f can be continued on $[0, T_I(x_0)+\bar{\epsilon}]$, [21]. Moreover, since $L_f H(\bar{x}) < 0$, for $\bar{\epsilon} > 0$ sufficiently small, $t_2 := T_I(x_0) + \bar{\epsilon}/2$ and $x_2 := \varphi^f(t_2, x_0)$, result in $H(x_2) < 0$. From $H(x_2) < 0$, it follows that $\mathrm{dist}(x_2, S) > 0$. If necessary, reduce $\bar{\epsilon}$ so that $0 < \bar{\epsilon} < \min\{\epsilon, T_I(x_0)\}$, and define $t_1 := T_I(x_0) - \bar{\epsilon}/2$ and $x_1 := \varphi^f(t_1, x_0)$. From

(61), $\mu(t_1) > 0$. From H2, the solutions depend continuously on the initial conditions. Thus, there exists $\delta > 0$, such that, for all $x \in B_\delta(x_0)$, $\sup_{0\le t\le t_2} ||\varphi^f(t,x) - \varphi^f(t,x_0)|| < \min\{\text{dist}(x_2, S), \mu(t_1)/2\}$. Therefore, for $x \in B_\delta(x_0)$, $t_1 < T_I(x) < t_2$, which implies that $|T_I(x) - T_I(x_0)| < \epsilon$, establishing the continuity of T_I at x_0. ■

Distance of a trajectory to a periodic orbit

Recall that if $\mathcal{O}$ is any periodic orbit that is transversal to S, then $\mathcal{O} \subset \tilde{\mathcal{X}}$. For $x \in \tilde{\mathcal{X}}$, define $d(x) := \sup_{0\le t\le T_I(x)} \text{dist}(\varphi^-(t,x), \mathcal{O})$. Note that d vanishes on $\mathcal{O}$. Note also that for $0 \le t \le T_I(x)$, $\varphi^-(t,x) = \varphi^f(t,x)$.

Lemma 4: Under H1-H3, $d : \tilde{\mathcal{X}} \to I\!R$ is well-defined and is continuous on $\mathcal{O}$.

Proof: For any $x_0 \in \tilde{\mathcal{X}}$, $T_I(x_0)$ is finite, and $\varphi^f(t,x_0)$ is defined on $[0, T_I(x_0)]$. This and the continuity of $\varphi^f(t,x_0)$ with respect to t imply that $d(x_0)$ is finite. Next, let $x_0 \in \mathcal{O}$ and $\epsilon > 0$ be given. By definition of T_I, $\bar{x} := \varphi^f(T_I(x_0), x_0) \in S$. Without loss of generality, suppose that $L_f H(\bar{x}) < 0$. Let $\eta > 0$ be such that for all $0 < t < \eta$, $H(\varphi^f(t,\bar{x})) < 0$ and $||\bar{x} - \varphi^f(t,\bar{x})|| < \epsilon/2$. Such an η exists because: (1) H1 implies there exists $\eta > 0$ such that φ^f can be continued on $[0, T_I(x_0) + \eta]$, [21]; (2) $L_f H(\bar{x}) < 0$; and (3) $\varphi^f(t,\bar{x})$ depends continuously on t. Define $t_3 := T_I(x_0) + \eta$ and $x_3 := \varphi^f(t_3, x_0)$. By H2 and Lemma 3, there exists $\delta > 0$ such that for all $\tilde{x} \in B_\delta(x_0)$, $\sup_{0\le t\le t_3} ||\varphi^f(t,x_0) - \varphi^f(t,\tilde{x})|| < \epsilon/2$ and $T_I(\tilde{x}) < t_3$. By the triangle inequality, $\text{dist}(\varphi^f(t,\tilde{x}), \mathcal{O}) \le \text{dist}(\varphi^f(t,\tilde{x}), \varphi^f(t,x_0)) + \text{dist}(\varphi^f(t,x_0), \mathcal{O})$. Hence, for $\tilde{x} \in B_\delta(x_0)$, $\sup_{0\le t\le T_I(\tilde{x})} \text{dist}(\varphi^f(t,\tilde{x}), \mathcal{O}) \le \sup_{0\le t\le t_3} \text{dist}(\varphi^f(t,\tilde{x}), \varphi^f(t,x_0)) + \sup_{0\le t\le t_3} \text{dist}(\varphi^f(t,x_0), \mathcal{O}) \le \epsilon/2 + \epsilon/2$, which shows that $d(\tilde{x}) \le \epsilon$, and thereby the continuity of d at x_0.

■

Proof of Theorem 1

Proof: The first and second statements are immediate. Since the sufficiency portions of the statement c) and d) are straightforward, only necessity is proven here. Suppose that $P(x_0) = x_0$, and let $\mathcal{O}$ be the periodic orbit of (11) corresponding to $\Delta(x_0)$. By b), the orbit is transversal to S. Let $\epsilon > 0$ be given. Since x_0 is stable in the sense of Lyapunov, for any $\bar{\epsilon} > 0$, there exists $\delta(\bar{\epsilon}) > 0$ such that, for all $k \ge 0$, $\bar{x} \in B_{\delta(\bar{\epsilon})}(x_0) \cap S$, implies $P^k(\bar{x}) \in B_\epsilon(x_0) \cap S$, where P^k is P composed with itself k-times. In particular, this implies that for all $\bar{x} \in B_{\delta(\bar{\epsilon})}(x_0) \cap S$, there exists a solution $\varphi(t)$ of (11) defined on $[0, \infty)$, such that $\varphi(0) = \Delta(\bar{x})$. Moreover, an upper bound on how far the solution φ

wanders from the orbit $\mathcal{O}$ is given by

$$\sup_{t\geq 0} \operatorname{dist}(\varphi(t),\mathcal{O}) \leq \sup_{x\in B_{\bar{\epsilon}}(x_0)\cap S} d\circ\Delta(x). \tag{62}$$

By Lemma 4, since $\mathcal{O}$ is transversal to S, and since $\Delta(x_0)\in\mathcal{O}$, $d\circ\Delta$ is continuous at x_0. Since $d\circ\Delta(x_0)=0$, it follows that there exists $\bar{\epsilon}>0$ such that $\sup_{x\in B_{\bar{\epsilon}}(x_0)\cap S} d\circ\Delta(x)<\epsilon$. This bound is valid for all initial conditions in $B_{\delta(\bar{\epsilon})}(x_0)\cap S$. It remains to produce an open neighborhood of $\mathcal{O}$ for which such a bound holds. But this is easily done by taking $\mathcal{V}:=d^{-1}([0,\delta))$, which completes the proof of c). Assume in addition that $\delta(\bar{\epsilon})>0$ was chosen sufficiently small so that $\lim_{k\to\infty} P^k(\bar{x})=x_0$. Then by continuity of d and Δ, $\lim_{k\to\infty} d\circ\Delta(P^k(\bar{x}))=d\circ\Delta(x_0)=0$, from which it easily follows that $\lim_{t\to\infty}\operatorname{dist}(\varphi(t),\mathcal{O})=0$, proving d).

■

Sufficient conditions for H1-H2

The goal is to show that the continuity of the feedback (22) plus Hypotheses CH1-CH3 imply that Hypotheses H1 and H2 hold for (24). H1 is immediate. Due to the subgroup property of the flow of a differential equation, it is enough to establish H2 in a local coordinate chart. Since (2) comes from the second order model, (1), where the matrix B is constant, the input vector fields of (2) commute and the dimension of their span is constant. These two facts plus the invertibility of the decoupling matrix (Hypothesis CH1) imply that, about any point $x_0\in\mathcal{X}$, the system (24) can be locally transformed into [26], [33], [37]

$$\begin{aligned}\dot{\zeta}_1 &= \zeta_2\\ \dot{\zeta}_2 &= \Psi(\zeta_1,\zeta_2)\\ \dot{z} &= \Gamma(\zeta_1,\zeta_2,z),\end{aligned} \tag{63}$$

where $\zeta_1:=y$, $\zeta_2:=\dot{y}$, Ψ is given by (22) and Γ is an analytic function of its arguments (the analyticity comes from that of (1)). In particular, Γ is locally Lipschitz continuous.

Thus, in these coordinates, the system is expressed as a cascade of a system that satisfies H2 feeding forward into a system that is locally Lipschitz. The Gronwal inequality [30] can therefore be easily used to establish that H2 holds for the cascade. This is summarized in the lemma below.

Lemma 5: For the closed-loop system (24), Hypotheses CH1-CH3 and the continuity of (22) imply Hypotheses H1 and H2.

TABLE I

RESULT OF OPTIMIZING THE CHOICE OF OUTPUTS FOR MINIMAL ENERGY CONSUMPTION.

i	a_0^i	a_1^i	a_2^i	a_3^i	$\hat{J}$
Original Values					
1	0.523	0	0	0	1,360
2	0	0	0	0	
Optimized Values					
1	0.512	0.073	0.035	-0.819	761
2	-2.27	3.26	3.11	1.89	

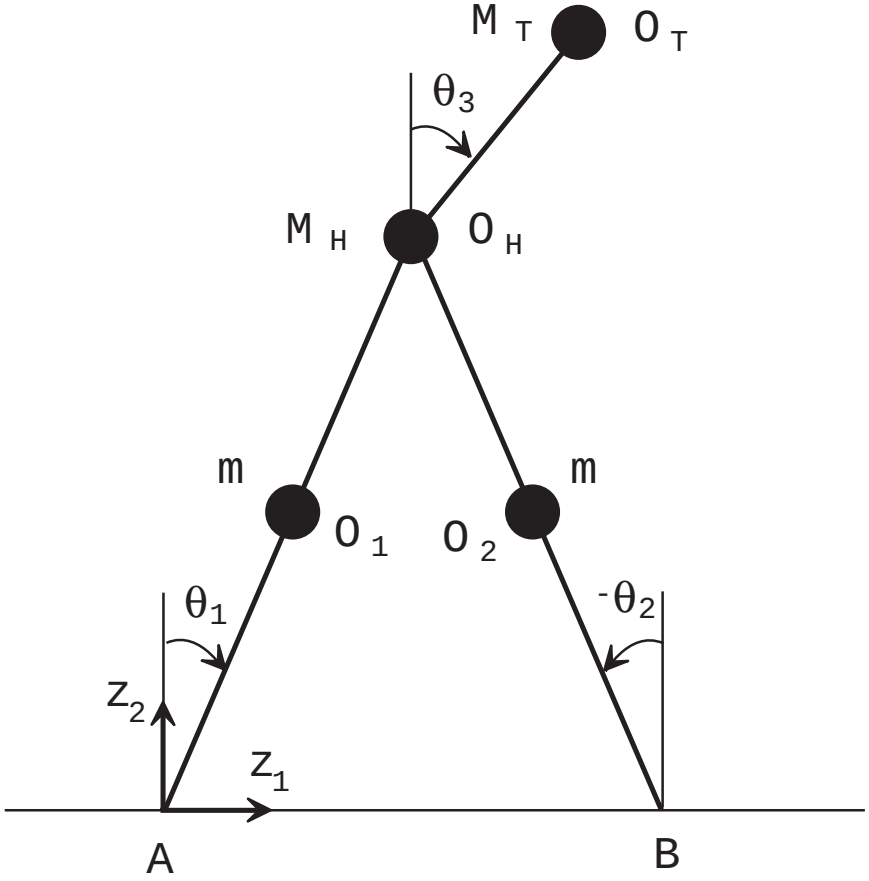

Fig. 1. Schematic indicating the defintion of the generalized coordinates and the mechanical data of the biped robot. All masses are lumped. The legs are symmetric, with length r equal to the length of the line segment $A - O_H$(also, $B - O_H$). The mass of each leg is lumped at $r/2$. The distance from the center of gravity of the hips to the center of gravity of the torso, denoted by l, is the distance from O_H to O_T.

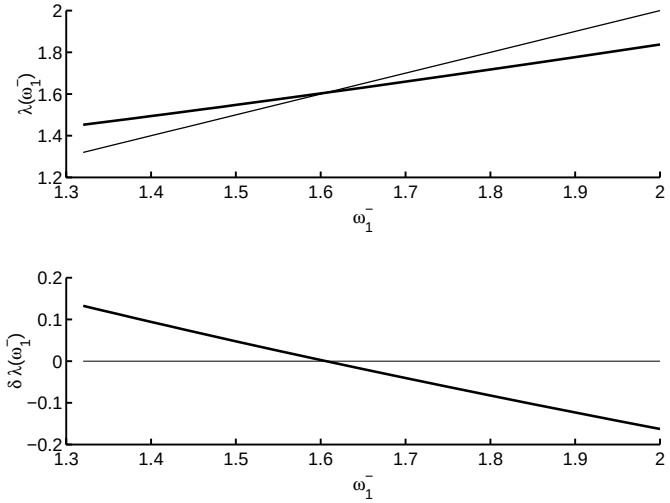

Fig. 2. The top graph presents the function λ (bold line) and, for visualization purposes, the identity function (thin line); the bottom graph presents the function $\delta\lambda$ (bold line) and the zero line (thin line). From either graph, it is seen that there exists a periodic orbit and that it is asymptotically stable.

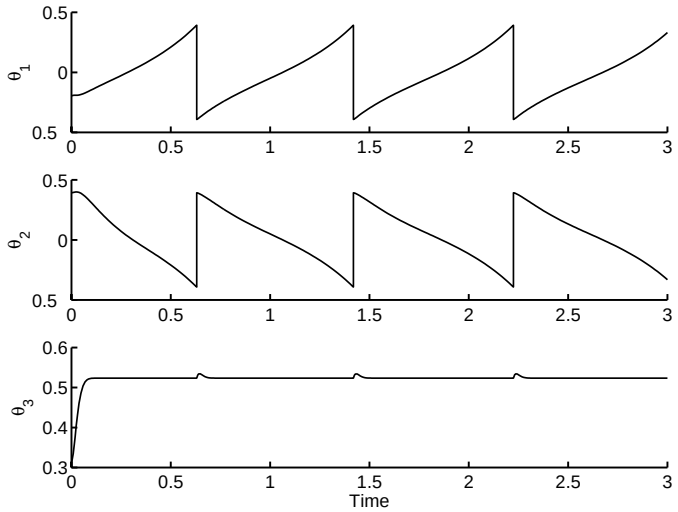

Fig. 3. Plot of joint angles versus time for a finite-time feedback computed on the basis of (15); units of radians.

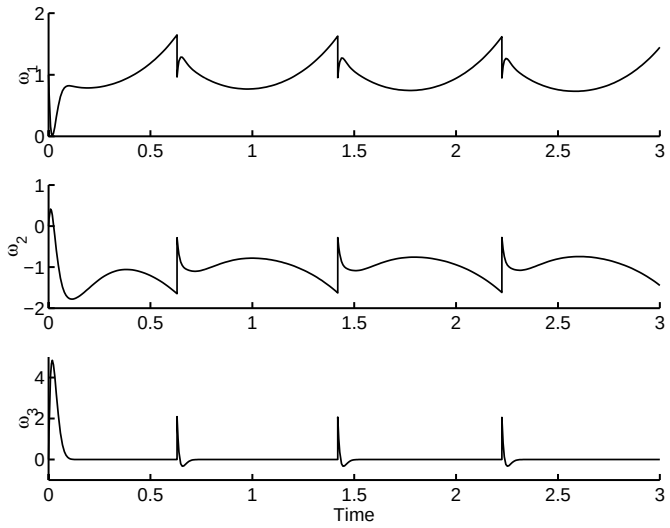

Fig. 4. Plot of joint velocities versus time for a finite-time feedback computed on the basis of (15); units of radians per second.

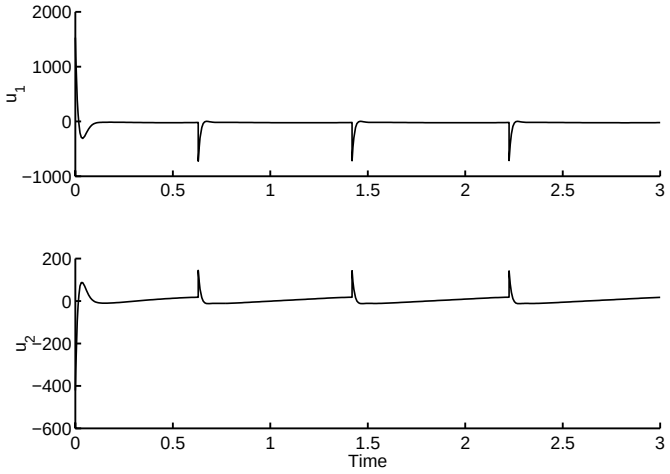

Fig. 5. Plot of applied torques versus time for a finite-time feedback computed on the basis of (15); units of newton-meters.

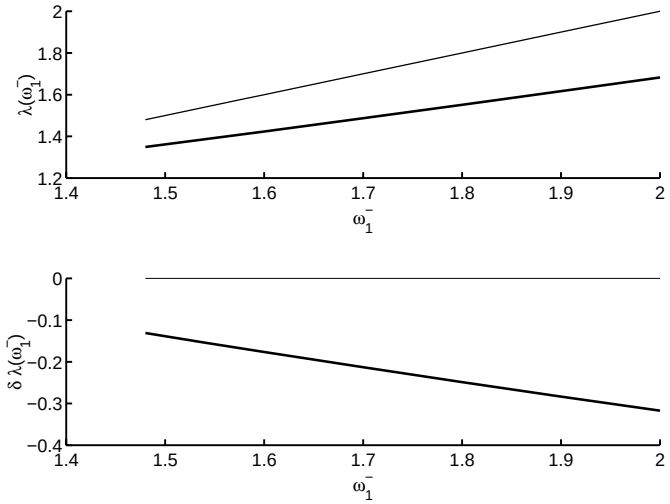

Fig. 6. The top graph presents the function λ (bold line) and, for visualization purposes, the identity function (thin line); the bottom graph presents the function $\delta\lambda$ (bold line) and the zero line (thin line). From either graph, it is seen that there does not exist a periodic orbit transversal to $\hat{S}$.

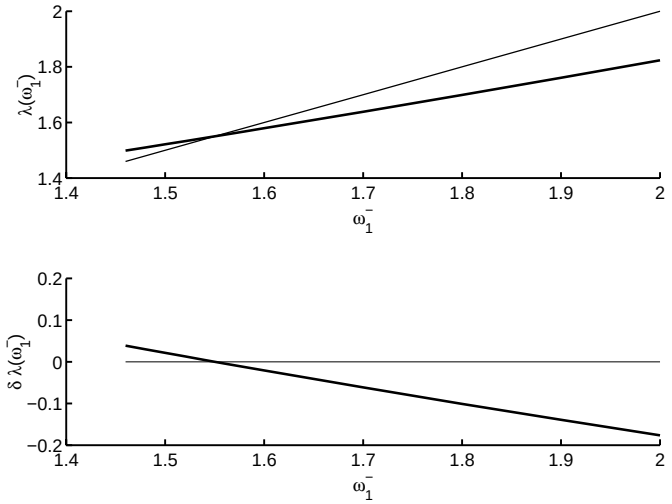

Fig. 7. The top graph presents the function λ (bold line) and, for visualization purposes, the identity function (thin line); the bottom graph presents the function $\delta\lambda$ (bold line) and the zero line (thin line). From either graph, it is seen that there exists a periodic orbit and that it is asymptotically stable.

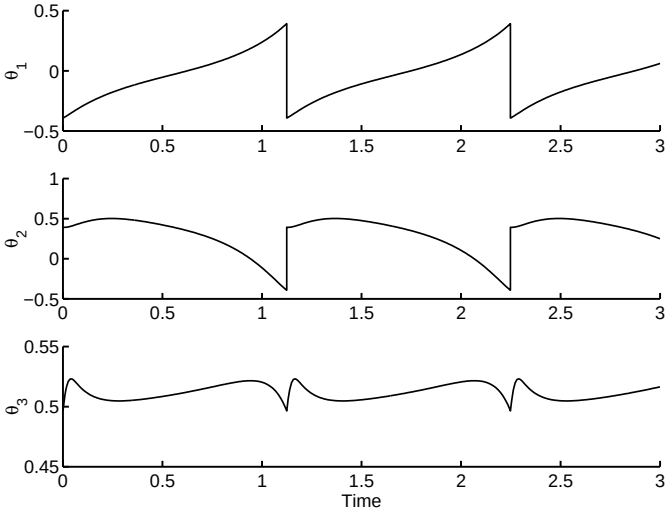

Fig. 8. Plot of joint angles versus time for a finite-time feedback computed on the basis of (34)-(35); units of radians.

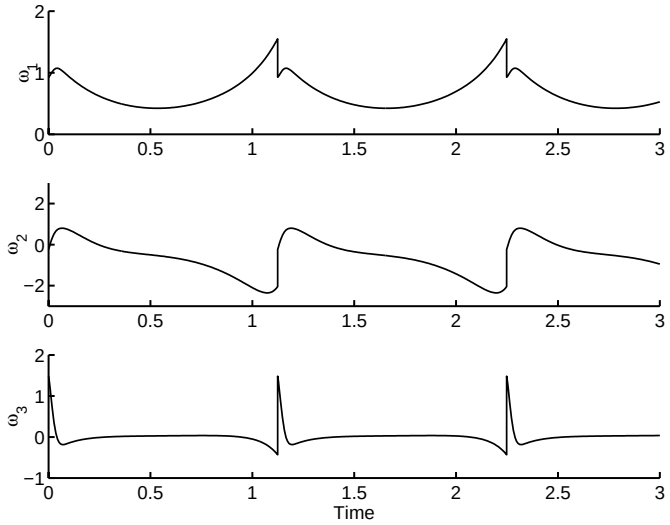

Fig. 9. Plot of joint velocities versus time for a finite-time feedback computed on the basis of (34)-(35); units of radians per second.

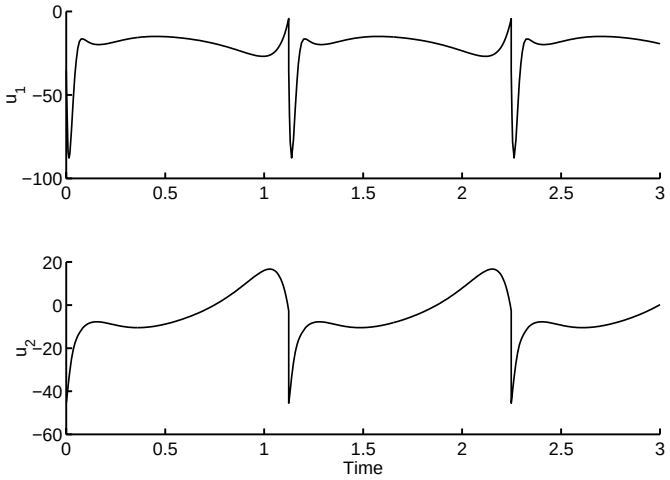

Fig. 10. Plot of applied torques versus time for a finite-time feedback computed on the basis of (34)-(35); units of newton-meters.